

R. & M. No. 3536



MINISTRY OF TECHNOLOGY

AERONAUTICAL RESEARCH COUNCIL
REPORTS AND MEMORANDA

Whirl of an Aircraft Power-plant Installation and its
Interaction with the Flutter Motion of a Flexible
Wing

By G. E. Smith

LONDON: HER MAJESTY'S STATIONERY OFFICE
1968
PRICE £1 2s. 6d. NET

Whirl of an Aircraft Power-plant Installation and its Interaction with the Flutter Motion of a Flexible Wing

By G. E. Smith

*Reports and Memoranda No. 3636**
August, 1966

Summary.

Results of propeller whirl analyses in four degrees of freedom are presented for a typical turbo-prop aircraft power-plant installation consisting of a rigid engine supported with elastically restrained freedoms in pitch and yaw at the end of a flexible nacelle cantilevered from a rigid support structure. Calculations were made for a range of structural and aerodynamic parameters. Only one of the four modes was found to become unstable within the airspeed range covered, the critical whirl airspeed being very sensitive to engine-mount damping and to the nacelle and engine-mount stiffnesses.

The interaction between power-plant whirl and wing flutter was investigated by extending the calculations to include twelve degrees of freedom, four normal modes of vibration of the half wing plus four modes for each of two power-plant installations on the half wing. The results suggest that the stability of the power-plant whirl modes is not adversely affected by motion of the wing, but that in certain circumstances the critical airspeed for wing flutter may be reduced slightly by a coupling with an unstable power-plant whirl mode of comparable frequency.

LIST OF CONTENTS

1. Introduction
2. Theory
 - 2.1. Form of the flutter equations
 - 2.2. System of generalised co-ordinates
 - 2.3. Partitioning of the flutter matrices
 - 2.4. Scaling of the flutter equations
 - 2.5. Solution of the flutter equations
3. Assembly of the Flutter Matrices
 - 3.1. Intertia Matrix [A]
 - 3.2. Structural stiffness matrix [E]
 - 3.3. Damping matrix [D]
 - 3.4. Aerodynamic damping and stiffness matrices [B] and [C]

*Replaces R.A.E. Tech. Report No. 66 284—A.R.C. 28 926.

LIST OF CONTENTS—*continued*

4. The Motion of a Nacelle-engine Installation Mounted on a Rigid Wing
 - 4.1. Engine whirl in two degrees of freedom
 - 4.2. Whirl of the nacelle in two degrees of freedom
 - 4.3. Whirl of the complete engine-nacelle installation in four degrees of freedom
 - 4.4. Whirl in four degrees of freedom with gyroscopic effects neglected
 - 4.5. The effect of engine mount and nacelle stiffnesses on the whirl-mode shapes and frequencies
 - 4.6. The effects of engine-mount stiffness and damping on the critical whirl airspeed
5. The Whirling Motion of a Nacelle-engine Installation Mounted on a Flexible Wing
 - 5.1. Flutter of the wing with rigid engine installations
 - 5.2. Flutter of the wing plus flexible engine installations, with propeller aerodynamic and gyroscopic effects neglected
 - 5.3. Flutter of the wing plus flexible engine installations, with propeller aerodynamic and gyroscopic effects considered
 - 5.4. The effect of frequency coincidence between wing modes and power-plant whirl modes
6. Conclusions
 - 6.1. The nature of whirling motion
 - 6.2. Whirling motion of an engine installation in two degrees of freedom
 - 6.3. Whirling motion of an engine installation in four degrees of freedom
 - 6.4. The interaction between wing-flutter modes and power-plant whirl modes

List of Symbols

References

Appendix A Analysis of the whirl motion of an engine installation in two degrees of freedom

Table 1 Basic data for engine-nacelle installations, used in forming the flutter matrices

Table 2 Propeller data and aerodynamic derivatives

Illustrations—Figs. 1 to 25

Detachable Abstract Cards

1. *Introduction.*

It is well known that a flexibly mounted propeller/power-plant installation can develop a self-excited motion characterised by a precession of the shaft with the propeller hub describing an elliptical path. This type of motion, known as ‘propeller whirl’, involves a coupling between the gyroscopic and aerodynamic forces acting on the propeller and rotating engine parts and the inertial, elastic and damping forces contributed by the power plant, nacelle and aircraft wing.

Under unfavourable combinations of aerodynamic excitation and inertia, flexibility, and damping of the engine mounts and nacelle structure, this whirl motion may become divergent, leading to failure of the engine-support structure and possibly to premature flutter of the entire wing. Such instability was not

encountered with the older piston-engined aircraft, but in recent turbo-prop engine configurations with large propellers and long overhanging nacelles, coupled with the higher airspeeds of turbo-prop aircraft, an unstable whirl motion is more liable to develop.

Reed and Bland¹ have presented a stability analysis of a flexibly mounted engine-propeller installation in two degrees of freedom only, namely pitch and yaw about a gimbal mounting. No allowance was made for nacelle flexibility or response of the wing. The results indicated that stability of the power-plant whirl motion is strongly dependent on the stiffness and damping in the mount system. Wind-tunnel tests³ on a model of a typical turbo-prop power plant, with freedoms in pitch and yaw only, have shown good agreement for whirl-mode frequencies and critical whirl airspeeds with calculated values using measured propeller aerodynamic derivatives. Further wind-tunnel tests⁴ on a complete model of a four-engined turbo-prop aircraft suggested that the flexibility of the wings may have a stabilizing effect on the whirl motion of the individual power plants, especially the inboard installations.

The present investigation was undertaken with the following objectives:

(1) To extend the whirl analysis of a power-plant installation to four degrees of freedom by including nacelle flexibilities as well as the engine mount freedoms, and to compare the results with those obtained from binary analyses.

(2) To examine the influence of nacelle and engine-mount stiffnesses and structural damping on the critical whirl airspeed of a power plant installation mounted on a rigid structure.

(3) To investigate the interaction between the flutter of a flexible half-wing and the whirl motions of two power-plant installations mounted on it by analysing the complete system in twelve degrees of freedom, four for each power plant and four for the half-wing.

The analyses were carried out on a Mercury digital computer using a standard flutter analysis programme. Basic data for the problem, such as the stiffness, inertia and aerodynamic matrices for the wing, were taken from a typical four-engined turbo-prop aircraft. The stiffnesses and structural dampings of the nacelle structures and engine mountings were varied over a range typical of values for modern turbo-prop aircraft.

2. Theory.

2.1. Form of the Flutter Equations

The equations of motion of the system are derived from Lagrange's equation:

$$\frac{d}{dt} \left(\frac{\partial \mathfrak{J}}{\partial \dot{q}_i} \right) - \frac{\partial \mathfrak{J}}{\partial q_i} + \frac{\partial \mathcal{D}}{\partial \dot{q}_i} + \frac{\partial U}{\partial q_i} = Q_i \quad (1)$$

where \mathfrak{J} is the kinetic energy

U is the potential energy

\mathcal{D} is the energy dissipated in damping

Q_i is the generalised force in the i^{th} mode

q_i is the generalised co-ordinate in the i^{th} mode.

The final equations of motion in the n degrees of freedom may be expressed in matrix form:

$$[A] \{ \ddot{q} \} + (\rho V [B] + [D]) \{ \dot{q} \} + (\rho V^2 [C] + [E]) \{ q \} = 0 \quad (2)$$

where $[A]$ is the inertia matrix of order $n \times n$

$[B]$ is the aerodynamic damping matrix containing contributions from the wing and propellers

$[C]$ is the aerodynamic stiffness matrix

$[D]$ is the damping matrix containing terms arising from structural damping and engine gyroscopic effects

$[E]$ is the structural stiffness matrix

$\{q\}$ is a column matrix of the n generalised co-ordinates

ρ is the air density (slug/ft³)

V is the true airspeed (ft/sec)

The dot notation is used to represent differentiation with respect to time.

2.2. System of Generalised Co-ordinates.

For the analysis of the complete half-wing of a typical four-engined turbo-prop aircraft twelve degrees of freedom are considered, four for each of the two engine installations and four for the wing structure itself.

In the installation upon which the analysis is based the engine itself is mounted on a tubular frame carried on a monocoque nacelle structure cantilevered from the wing. The engine is attached to the tubular frame by flexible rubber mounts which allow it to rotate in pitch and yaw relative to the frame as if it were mounted in gimbals. The geometry of the engine-nacelle installation is shown in Fig. 1.

The modes of deformation assumed for the complete nacelle-engine installation are shown in Fig. 2. The two degrees of freedom chosen for the engine are the pitching and yawing rotations (α_1 and β_1 respectively) of the engine about an effective gimbal mounting, measured relative to the tangent at the nacelle tip. The two freedoms allowed to the nacelle are the vertical and horizontal displacements (z_1 and y_1) of the gimbal point G , relative to the tangent at the nacelle root. The nacelle is assumed to behave as a cantilever and to deflect both vertically and horizontally into parabolic curves. This introduces pitching and yawing rotations at the nacelle tip which augment the rotations of the engine and thus introduce inertia and aerodynamic coupling between the engine and nacelle freedoms. The additional displacements z_w and θ_w (Fig. 2) are, respectively, the vertical deflection of the wing flexural axis and the pitching rotation of the wing about it, measured at the engine station relatively to a datum at the wing root.

The four generalised co-ordinates allocated to the wing are associated with four of the antisymmetric normal modes of the aircraft calculated with the aerodynamic and gyroscopic forces arising from the propellers and engines neglected. The four wing mode shapes considered will be described later in Section 5.

The twelve generalised co-ordinates associated with the half-wing and two power-plant installations may be written as a column matrix partitioned thus:

$$\{q\} = \begin{Bmatrix} q_w \\ - \\ q_{NI} \\ - \\ q_{NO} \end{Bmatrix}$$

$\{q_w\}$ is a column matrix composed of the four wing co-ordinates.

$$\{q_{NI}\} = \begin{Bmatrix} z_1 \\ \alpha_1 \\ y_1 \\ \beta_1 \end{Bmatrix}$$

where z_1 , α_1 , y_1 and β_1 are the four generalised co-ordinates associated with the inboard power plant installation.

$\{q_{NO}\}$ is a column matrix composed of the four generalised co-ordinates associated with the outboard power plant.

2.3. Partition of the Matrices.

Following the system of partitioning adopted for the twelve generalised co-ordinates the matrices are partitioned in the same way. For example the inertia matrix $[A]$ may be written

$$[A] = \begin{bmatrix} A_{WW} & A_{WI} & A_{WO} \\ - & - & - \\ A_{IW} & A_{II} & A_{IO} \\ - & - & - \\ A_{OW} & A_{OI} & A_{OO} \end{bmatrix}$$

where the subscripts W , I and O refer to the wing, inboard engine installation and outboard engine installation respectively.

With this system of co-ordinates there is no coupling between the two engine installations, i.e. $A_{IO} = A_{OI} = 0$. Coupling does however exist between the wing and engine freedoms, with both installations contributing to the sub-matrix A_{WW} , as shown in Section 3.1.1. The other matrices B , C , D and E are partitioned in a similar manner.

2.4. Scaling of the Flutter Equations.

The following form of overall scaling is adopted, the factors being applied to every term in the appropriate matrices.

$$\left. \begin{array}{l} [a] = [A]/\rho_0 c_m^2 \\ [b] = [B]/c_m \\ [c] = [C] \\ [d] = [D]/\rho_0 V_0 c_m \\ [e] = [E]/\rho_0 V_0^2 \end{array} \right\} \quad (3)$$

In addition the following dimensionless quantities are introduced:

$$\text{Dimensionless airspeed } v = V/V_0$$

$$\text{Dimensionless air density } \sigma = \rho/\rho_0$$

$$\text{Dimensionless time } \tau = t V_0/c_m$$

where ρ_0 is the air density at sea level

V_0 is a reference airspeed

c_m is a reference length such as the wing mean chord.

After substituting these expressions into equation (2) the flutter equation is obtained in the matrix form

$$[a] \{\ddot{q}\} + (\sigma v [b] + [d]) \{\dot{q}\} + (\sigma v^2 [c] + [e]) \{q\} = 0 \quad (4)$$

where the dash notation here represents differentiation with respect to dimensionless time τ .

2.5. Solution of the Flutter Equations.

The flutter equations may be solved numerically for given values of v and σ by means of a programme written for the digital computer Mercury. The results obtained are the real and imaginary parts μ_r and ω_r of the complex latent roots λ_r of the scaled flutter determinant formed from equation (4).

The frequency and decay rate of the r^{th} mode of vibration are then given by:
Frequency

$$\omega_r = \omega_r' (V_0/c_m) \text{ rad/sec} \quad (5a)$$

Decay rate, as a fraction of the critical value

$$\zeta_r = \mu_r' / (\mu_r'^2 + \omega_r'^2)^{\frac{1}{2}} \quad (5b)$$

Using the values of μ_r' and ω_r' obtained from the flutter programme the complex ratios between the vectors associated with each of the degrees of freedom contributing to the r^{th} mode of vibration can be found from a subsidiary programme. From the amplitude ratios and phase relationships between the vectors the displacements of the various parts of the structure may be determined for each mode.

3. Assembly of the Matrices.

3.1. Inertia Matrix $[A]$.

The inertia matrix is made up of contributions from the engines, nacelles and aircraft wing.

3.1.1. *Inertia effects of engines.* The kinetic energy of an engine, arising from its vertical and horizontal translations and its pitching and yawing rotations about the gimbal mounting, may be expressed in matrix form in terms of its mass and moments of inertia and the displacements of its c.g.

$$\mathfrak{I}_E = \frac{1}{2} [\dot{z}_E, \dot{\theta}, \dot{y}_E, \dot{\psi}] [M_E] \{z_E, \theta, y_E, \psi\} \quad (6)$$

where $[M_E]$ is the diagonal matrix

$$\begin{bmatrix} m_E & 0 \\ I_\theta & \\ & m_E \\ 0 & I_\psi \end{bmatrix} \quad (7)$$

and $[\]$ denotes a row matrix, $\{ \ } \}$ a column matrix.

The displacements of the engine c.g. are related to the generalised co-ordinates associated with the nacelle-engine installation and the displacements of the wing flexural axis by the matrix transformation.

$$\{z_E, \theta, y_E, \psi\} = [T_{WE} | T_E] \{z_W, \theta_W | q_N\} \quad (8)$$

where $\{q_N\}$ is the column matrix $\{z_1, \alpha_1, y_1, \beta_1\}$.

The matrices $[T_{WE}]$ and $[T_E]$ may be written down from inspection of Fig. 2.

$$[T_{WE}] = \begin{bmatrix} 1 & -x_E \\ 0 & 1 \\ 0 & 0 \\ 0 & 0 \end{bmatrix} \quad (9)$$

$$[T_E] = \begin{bmatrix} (1+r_\theta l_E) & -l_E & 0 & 0 \\ -r_\theta & 1 & 0 & 0 \\ 0 & 0 & (1+r_\psi l_E) & l_E \\ 0 & 0 & r_\psi & 1 \end{bmatrix} \quad (10)$$

The displacements z_w and θ_w are related to the generalised co-ordinates associated with the wing by the transformation

$$\{z_w, \theta_w\} = [\Delta_w] \{q_w\} \quad . \quad (11)$$

The numerical values of the coefficients of the 2×4 matrix $[\Delta_w]$ may be found by interpolation from the modal column matrices of wing displacements in the four wing modes selected.

After combining equations (6), (8) and (11) and substituting into equation (1) the contribution of the engine installation to the Lagrangian equation is found to be

$$\frac{d}{dt} \left(\frac{\partial \mathfrak{J}_E}{\partial \dot{q}_i} \right) - \frac{\partial \mathfrak{J}_E}{\partial q_i} = \begin{bmatrix} [\Delta_w]' [T_{WE}]' [M_E] [T_{WE}] [\Delta_w] & [\Delta_w]' [T_{WE}]' [M_E] [T_E] \\ \hline \hline [T_E]' [M_E] [T_{WE}] [\Delta_w] & [T_E]' [M_E] [T_E] \end{bmatrix} \begin{Bmatrix} \ddot{q}_w \\ \ddot{q}_N \end{Bmatrix} \quad . \quad (12)$$

The resulting matrix is of order 8×8 and may be partitioned into the four wing freedoms and the four freedoms of the engine-nacelle installation as shown. The inertia contributions from both engine installations are calculated from equation (12) and are added into the full 12×12 inertia matrix according to the partitioning scheme described in Section 2.3.

3.1.2. Inertia effects of the nacelles. Each nacelle is represented by a set of concentrated masses distributed along its length, and is assumed to vibrate in parabolic modes in the (x,z) and (x,y) planes, as described in Section 2.

The kinetic energy of the nacelle may be written in matrix form as

$$\mathfrak{J}_N = \frac{1}{2} [\dot{z}_N \quad | \quad \dot{y}_N] [M_N] \{\dot{z}_N \quad | \quad \dot{y}_N\} \quad (13)$$

$\{y_N\}$ and $\{z_N\}$ are column sub-matrices whose n^{th} elements represent the displacements of the n^{th} concentrated nacelle mass in the y and z directions respectively.

$[M_N]$ is the diagonal matrix whose elements are the concentrated nacelle masses associated with the elements of the displacement matrices $\{y_N\}$ and $\{z_N\}$.

The displacement column matrix $\{z_n \quad | \quad y_N\}$ may be expressed in terms of the displacements z_w and θ_w at the wing flexural axis, and the column matrix $\{q_N\}$ of the nacelle freedoms by the transformation

$$\{z_N \quad | \quad y_N\} = [T_{WN} \quad | \quad T_N] \{z_w, \theta_w \quad | \quad q_N\} \quad . \quad (14)$$

From inspection of Fig. 2 the transformation matrices may be written as

$$[T_{WN}] = \begin{bmatrix} 1, & x_1 \\ 1, & x_2 \\ \vdots & \vdots \\ 1, & x_n \\ \hline \hline 0 & \end{bmatrix} \quad (15)$$

and

$$[T_N] = \begin{bmatrix} \left(\frac{x_1 - x_L}{l}\right)^2, & 0 & 0 & 0 \\ \left(\frac{x_2 - x_L}{l}\right)^2, & 0 & 0 & 0 \\ \vdots & \vdots & \vdots & \vdots \\ \left(\frac{x_n - x_L}{l}\right)^2, & 0 & 0 & 0 \\ \hline 0 & 0 & \left(\frac{x_1 - x_L}{l}\right)^2 & 0 \\ 0 & 0 & \left(\frac{x_2 - x_L}{l}\right)^2 & 0 \\ \vdots & \vdots & \vdots & \vdots \\ 0 & 0 & \left(\frac{x_n - x_L}{l}\right)^2 & 0 \end{bmatrix} \quad (16)$$

where x_n is the distance of the n^{th} concentrated mass from the wing flexural axis, and x_L is the distance of the nacelle 'root' from the flexural axis.

After combining equations (13), (14) and (11) the contribution of the nacelle to the Lagrangian equation becomes

$$\frac{d}{dt} \left(\frac{\partial \mathfrak{I}_N}{\partial \dot{q}_i} \right) - \frac{\partial \mathfrak{I}_N}{\partial q_i} = \begin{bmatrix} [\Delta_w]' [T_{WN}]' [M_N] [T_{WN}] [\Delta_w] & [\Delta_w]' [T_{WN}]' [M_N] [T_N] \\ \hline [T_N]' [M_N] [T_{WN}] [\Delta_w] & [T_N]' [M_N] [T_N] \end{bmatrix} \begin{Bmatrix} \ddot{q}_w \\ \ddot{q}_N \end{Bmatrix} \quad (17)$$

This is a matrix of order 8×8 and is added into the full 12×12 inertia matrix in a similar manner to the engine contribution.

3.1.3. Inertia effects of wing. The wing is treated as a set of concentrated masses and moments of inertia distributed along its span. Four generalised co-ordinates, each associated with an antisymmetric normal mode of vibration, are allocated to the wing.

The contribution of the wing to the inertia matrix is evaluated in a similar manner to that of the nacelles, by forming the matrix products from the wing mass and moment of inertia matrix and the displacement matrix derived from the four modal columns. In this case however the elements of the modal columns were obtained from previous normal mode calculations carried out on the wing, plus engine installations having freedom in the vertical plane only.

3.2. The Structural-stiffness Matrix [E].

The structural-stiffness matrix is made up of contributions from the wing structure itself and from the two engine installations.

3.2.1. Wing stiffness. The original stiffness data, obtained from a typical turbo-prop aircraft, was in the form of a diagonal matrix derived from a normal mode analysis of the complete wing, plus the two

original engine installations having freedoms in the vertical plane only. To allow for subsequent variations in the engine mount and nacelle stiffnesses, and the introduction of additional degrees of freedom into the engine installations, it was necessary to separate the stiffness effects of the original installations from the complete diagonal stiffness matrix, leaving the contribution arising from the wing itself.

For this purpose the following data were obtained:

- [E_T] The original diagonal stiffness matrix for the complete wing plus engine installations, expressed in terms of the four generalised co-ordinates $\{q_w\}$.
- [E_B] The stiffness matrix for each engine installation in terms of the arbitrary 'branch mode' co-ordinates $\{q_B\}$, originally used in the calculation of [E_T].
- [Z_0] The matrix composed of the four modal columns giving the displacement amplitudes of points on the wing and engines in the four normal modes of vibration, in terms of the co-ordinates $\{q_w\}$.

The displacements of n arbitrarily chosen points on the engine installation may be expressed in terms of the co-ordinates $\{q_w\}$ by extracting the n relevant rows from the modal matrix $[Z_0]$.

Thus

$$\{z_n\} = [Z_n] \{q_w\} \quad (18)$$

The same displacements may also be written in terms of the displacements z_w and θ_w of the wing flexural axis at the engine station, and of the branch mode co-ordinates $\{q_B\}$

$$\{z_n\} = [T_w \mid T_1] \{z_w, \theta_w \mid q_B\} \quad (19)$$

The matrices $[T_w]$ and $[T_1]$ may be determined directly from the geometry of the installation. Combining equations (18) and (19) we have:

$$\{z_w, \theta_w \mid q_B\} = [T_w \mid T_1]^{-1} [Z_n] \{q_w\} \quad (20)$$

It must be stressed that for this equation to have any meaning it is necessary for the matrix $[T_w \mid T_1]$ to be square. This condition may be satisfied by taking n to be greater by two than the number of branch mode co-ordinates $\{q_B\}$.

The co-ordinates $\{q_B\}$ and $\{q_w\}$ are related by a transformation matrix $[T_B]$, yet to be found

$$\{q_B\} = [T_B] \{q_w\} \quad (21)$$

After combining equations (11) and (21) the left hand side of equation (20) can be written in the partitioned form:

$$\{z_w, \theta_w \mid q_B\} = \left[\frac{\Delta_w}{T_B} \right] \{q_w\} \quad (22)$$

Hence by comparison of equations (20) and (22) the following identity is obtained:

$$\left[\frac{\Delta_w}{T_B} \right] \equiv [T_w \mid T_1]^{-1} [Z_n] \quad (23)$$

The matrix $[\Delta_w]$ is thus simply the first two rows of the expanded matrix product $[T_w \mid T_1]^{-1} [Z_n]$, while the transformation matrix $[T_B]$ is given by the remaining rows.

As a check on the accuracy of the above matrix manipulations the elements of $[\Delta_w]$ obtained from equation (23) may be compared with the values obtained by interpolation from the modal columns contained in $[Z_0]$. If agreement is poor, for example because of ill-conditioning in the matrix inversion, the calculations may be repeated using a different set of displacements z_n , provided of course that sufficient data are available from the modal matrix $[Z_0]$.

The transformation matrix $[T_B]$ having been found, the stiffness effects of the engine installations may be split off from the original diagonal stiffness matrix, to leave the contribution arising from the wing alone:

$$[E_{WW}] = [E_T] - |[T_B][E_B][T_B]|_I - |[T_B][E_B][T_B]|_O \quad (24)$$

where the subscripts I and O refer to the inboard and outboard installations respectively.

3.2.2. Stiffness of the engine-nacelle installations. The stiffness sub-matrix for the inboard engine installation in terms of the four generalised co-ordinates $\{q_N\}_I$ may be written as

$$[E_{II}] = \begin{bmatrix} K_z & 0 \\ K_\alpha & \\ K_\gamma & \\ 0 & K_\beta \end{bmatrix} \quad (25)$$

The stiffness matrix $[E_{OO}]$ for the outboard installation is similar in form.

The coefficients may either be calculated from a structural analysis of the installation or obtained experimentally. K_α and K_β represent the effective spring stiffnesses restraining pitching and yawing rotations of the engine about its gimbal mounting. K_z and K_γ are the translational stiffnesses of the nacelle cantilever in the vertical and horizontal planes, referred to the gimbal point G .

With the co-ordinate system employed there is no stiffness cross-coupling between the engine freedoms and the nacelle freedoms. In fact the choice of the degrees of freedom was partly influenced by the desire to obtain a stiffness matrix free from cross terms. In addition there is no coupling between the two engine installations and the wing.

The complete 12×12 stiffness matrix for the system may be written in the form

$$[E] = \left[\begin{array}{c|c|c} E_{WW} & 0 & 0 \\ \hline 0 & E_{II} & 0 \\ \hline 0 & 0 & E_{OO} \end{array} \right] \quad (26)$$

3.3. Damping Matrix $[D]$.

The damping matrix is made up of terms arising from structural damping inherent in the structure or deliberately introduced at the engine mountings, and terms arising from the gyroscopic effects of the propeller and rotating engine parts.

3.3.1. Structural damping. Viscous damping (i.e. damping force proportional to vibrational velocity) is assumed to act in the degrees of freedom of the engine installations only. The structural damping matrix for each installation is diagonal in form, the damping term in the i^{th} degree of freedom being

$$d_{ii} = 2\zeta_i(a_{ii}e_{ii})^{\frac{1}{2}} \quad (27)$$

where a_{ii} and e_{ii} are the direct inertia and stiffness terms in the i^{th} freedom, and ζ_i is the viscous damping coefficient expressed as a fraction of the critical damping.

3.3.2. Gyroscopic effects of propellers and engines. Due to the rotation of the propeller and moving engine parts an additional term appears in the expression for the kinetic energy of the system

$$\mathfrak{I}_G = \frac{1}{2} I_P \omega_P^2 \quad (28)$$

where I_P is the effective polar moment of inertia of the propeller and rotating engine parts, and ω_P is the total angular velocity of the propeller about the displaced axis of the propeller shaft.

With zero rolling motion, and for small total pitching and yawing rotations θ and ψ of the shaft (Fig. 2) we may write

$$\begin{aligned} \omega_P &\simeq \Omega + \dot{\theta} \sin \psi \\ &\simeq \Omega + \dot{\theta} \psi \end{aligned} \quad (29)$$

where Ω is the propeller rotational speed relative to the engine.

Therefore

$$\mathfrak{I}_G \simeq \frac{1}{2} I_P (\Omega^2 + 2\Omega \dot{\theta} \psi) \quad (30)$$

the term in ψ^2 being neglected.

The displacements of the c.g. of the engine plus propeller may be written as a column matrix $\{\delta\}$

$$\text{where } \{\delta\} = \{z_E, \theta, y_E, \psi\}.$$

The contribution to the Lagrangian equations may be evaluated in terms of these displacements as follows:

Displacement δ	$\frac{d}{dt} \left(\frac{\partial \mathfrak{I}_G}{\partial \delta} \right)$	$-\frac{\partial \mathfrak{I}_G}{\partial \delta}$
z_E	0	0
θ	$I_P \Omega \psi$	0
y_E	0	0
ψ	0	$-I_P \Omega \dot{\theta}$

In matrix form

$$\frac{d}{dt} \left(\frac{\partial \mathfrak{I}_G}{\partial \delta} \right) - \frac{\partial \mathfrak{I}_G}{\partial \delta} = [G] \{ \dot{z}_E, \dot{\theta}, \dot{y}_E, \dot{\psi} \} \quad (31)$$

where

$$[G] = I_P \Omega \begin{bmatrix} 0 & 0 & 0 & 0 \\ 0 & 0 & 0 & 1 \\ 0 & 0 & 0 & 0 \\ 0 & -1 & 0 & 0 \end{bmatrix} \quad (32)$$

The transformation matrices given in equations (9), (10) and (11) may now be used to express equation (31) in terms of the generalised co-ordinates $\{q_w\}$ and $\{q_N\}$

$$\frac{d}{dt} \left(\frac{\partial \mathfrak{J}_G}{\partial \dot{q}_i} \right) - \frac{\partial \mathfrak{J}_G}{\partial q_i} = \begin{bmatrix} [\Delta_W][T_{WE}]'[G][T_{WE}][\Delta_W] & [\Delta_W][T_{WE}]'[G][T_E] \\ [T_E]'[G][T_{WE}][\Delta_W] & [T_E]'[G][T_E] \end{bmatrix} \begin{Bmatrix} \dot{q}_W \\ \dot{q}_N \end{Bmatrix} \quad (33)$$

It may be noted that the kinetic energy of rotation of the engine and propeller gives a contribution to the Lagrangian equations in the form of a damping matrix rather than an inertia matrix. The same result would have been obtained by considering the work done by the gyroscopic moments arising from the pitching and yawing velocities $\dot{\theta}$ and $\dot{\psi}$ of the rotating parts, but the above approach via the kinetic energy of the system is simpler and less liable to errors in sign than an analysis using the classical equations of the gyroscope.

3.4. Aerodynamic Damping and Stiffness Matrices [B] and [C].

3.4.1. Aerodynamic forces and moments acting on propeller. The forces and moments acting upon a propeller rotating at incidence to the airstream may be resolved into the components F_z , F_y , M_θ and M_ψ , the positive directions of which are shown in Fig. 2. Each of these forces and moments consists of a steady value upon which is superimposed a small order fluctuating component depending on the number of propeller blades and other factors.

The steady parts of these forces and moments are given by the following expressions¹:

$$\left. \begin{aligned} F_z &= \frac{1}{2}\rho V^2 S (C_{z\theta} \bar{\theta} + C_{z\psi} \bar{\psi} + C_{zr} \dot{\theta} R/V) \\ M_\theta &= \rho V^2 S R (C_{m\psi} \bar{\psi} + C_{mq} \dot{\theta} R/V) \\ F_y &= \frac{1}{2}\rho V^2 S (C_{y\psi} \bar{\psi} + C_{y\theta} \bar{\theta} + C_{yr} \dot{\theta} R/V) \\ M_\psi &= \rho V^2 S R (C_{n\theta} \bar{\theta} + C_{nr} \dot{\psi} R/V) \end{aligned} \right\} \quad (34)$$

where $\bar{\theta}$ and $\bar{\psi}$ are the effective pitch and yaw angles of the propeller relative to the airstream:

$$\left. \begin{aligned} \bar{\theta} &= \theta + \dot{z}_p/V \\ \bar{\psi} &= \psi - \dot{y}_p/V \end{aligned} \right\} \quad (35)$$

R = propeller radius

S = area of propeller disc.

After substituting the above expressions for $\bar{\theta}$ and $\bar{\psi}$ equations (34) may be written in matrix form as

$$\begin{Bmatrix} F_z \\ M_\theta \\ F_y \\ M_\psi \end{Bmatrix} = \rho V^2 [F_C] \begin{Bmatrix} z_p \\ \theta \\ y_p \\ \psi \end{Bmatrix} + \rho V [F_B] \begin{Bmatrix} \dot{z}_p \\ \dot{\theta} \\ \dot{y}_p \\ \dot{\psi} \end{Bmatrix} \quad (36)$$

where

$$[F_C] = S \begin{bmatrix} 0 & \frac{1}{2} C_{z\theta} & 0 & \frac{1}{2} C_{z\psi} \\ 0 & 0 & 0 & R C_{m\psi} \\ 0 & \frac{1}{2} C_{y\theta} & 0 & \frac{1}{2} C_{y\psi} \\ 0 & R C_{n\theta} & 0 & 0 \end{bmatrix} \quad (37)$$

and

$$[F_B] = S \begin{bmatrix} \frac{1}{2} C_{z\theta} & 0 & -\frac{1}{2} C_{z\psi} & \frac{1}{2} R C_{zr} \\ 0 & R^2 C_{mq} & -R C_{m\psi} & 0 \\ \frac{1}{2} C_{y\theta} & \frac{1}{2} R C_{yq} & -\frac{1}{2} C_{y\psi} & 0 \\ R C_{n\theta} & 0 & 0 & R^2 C_{nr} \end{bmatrix} \quad (38)$$

The terms in \ddot{z}_P and \ddot{y}_P have been omitted since equations (34) are only applicable to steady flow and it is doubtful whether the acceleration terms arising from the differentiation of $\bar{\theta}$ and $\bar{\psi}$ have any validity. It is known however that such aerodynamic inertia effects are very small compared with the structural inertias and their omission is therefore justifiable.

The displacements of the propeller may be expressed in terms of the generalised co-ordinates by transformations similar to those of Section 3.1, i.e.

$$\{z_P, \theta, y_P, \psi\} = [T_{WP} \mid T_P] \{z_W, \theta_W \mid q_N\} \quad (39)$$

where $[T_{WP}] = \begin{bmatrix} 1 & -x_P \\ 0 & 1 \\ 0 & 0 \\ 0 & 0 \end{bmatrix} \quad (40)$

and

$$[T_P] = \begin{bmatrix} (1+r_\theta l_p) & -l_p & 0 & 0 \\ -r_\theta & 1 & 0 & 0 \\ 0 & 0 & (1+r_\psi l_p) & l_p \\ 0 & 0 & r_\psi & 1 \end{bmatrix} \quad (41)$$

Hence in terms of the co-ordinates $\{q_W\}$ and $\{q_N\}$ the generalised forces on the right hand side of the Lagrangian equation become:

$$\begin{Bmatrix} Q_W \\ Q_N \end{Bmatrix} = \rho V^2 \begin{bmatrix} [\Delta_W]' [T_{WP}]' [F_C] [T_{WP}] [\Delta_W] & [\Delta_W]' [T_{WP}]' [F_C] [T_P] \\ \hline [T_P]' [F_C] [T_{WP}] [\Delta_W] & [T_P]' [F_C] [T_P] \end{bmatrix} \begin{Bmatrix} q_W \\ q_N \end{Bmatrix} \quad (42)$$

$$+ \rho V \begin{bmatrix} [\Delta_W]' [T_{WP}]' [F_B] [T_{WP}] [\Delta_W] & [\Delta_W]' [T_{WP}]' [F_B] [T_P] \\ \hline [T_P]' [F_B] [T_{WP}] [\Delta_W] & [T_P]' [F_B] [T_P] \end{bmatrix} \begin{Bmatrix} \dot{q}_W \\ \dot{q}_N \end{Bmatrix}$$

The first and second terms on the right hand side of equation (42) represent, after a change in sign, the contributions of the propeller to the aerodynamic stiffness and damping matrices respectively of equation (2).

3.4.2. Evaluation of the propeller aerodynamic derivatives. The derivatives $C_{z\theta}$, $C_{z\psi}$ etc are calculated from the equations given by Ribner². The derivatives depend mainly on airspeed and propeller rotational speed, but are most conveniently calculated as functions of the advance ratio $J = V/2NR$.

Since the effect of propeller thrust on the values of the derivatives is known to be small¹ they are evaluated for a non-thrusting (windmilling) propeller. Numerical values are given in Table 2.

3.4.3. Aerodynamic effects of the wing. The aerodynamic damping and stiffness submatrices in terms of the four degrees of freedom of the wing were available from previous flutter calculations and were added directly into the matrices $[B]$ and $[C]$.

4. The Motion of a Nacelle-Engine Installation Mounted on a Rigid Wing.

Stability analyses in up to four degrees of freedom were carried out on a typical installation in order to examine the possibility of an unstable motion developing above a certain airspeed. All dimensions and mass data used were taken from an installation employed on a typical four-engined turbo-prop aircraft. The stiffness matrix coefficients were derived from early estimates of the stiffness of the nacelle and engine mounts of the installation. Structural damping of the 'viscous' type (force proportional to velocity) was assumed to act in the pitching and yawing freedoms of the engine relative to the nacelle. (Section 3.3.1). Aerodynamic and gyroscopic forces and moments arising from the propeller and rotating engine parts were evaluated at the maximum r.p.m. of the propeller at take-off for three values of the advance ratio J , as described in Section 3.4.1.

4.1. Engine Whirl in Two Degrees of Freedom.

In this analysis only the pitching and yawing rotational freedoms of the outboard engine relative to its nacelle were considered. A viscous-damping coefficient of 2 per cent of critical was assumed for each degree of freedom.

The frequencies and decay rates of the two resulting modes of vibration are shown in Fig. 3 as functions of the dimensionless airspeed v at sea level ($\sigma = 1$) for three values of advance ratio J . The modes are numbered in ascending order of frequency.

The nature of the motion in each of the modes is best understood by considering the complex vectors associated with the two latent roots of the binary flutter equations. The complex vectors for $v = 0$ are shown alongside their respective curves in Fig. 3, the usual right-handed vector sign convention being used.

In mode 1 the vector β_1 , (yawing rotation) lags vector α_1 (pitching rotation) by approximately 90 deg. With the sign convention adopted here the resulting motion of the propeller hub is an elliptical orbit in the y,z plane in an anticlockwise direction when viewed from ahead. This is in the opposite sense to the propeller rotation in this case and thus may be identified as the backward whirl mode of Appendix A.

In mode 2 the vector β_1 leads vector α_1 by approximately 90 deg, the resulting motion of the propeller hub being an elliptical orbit in the y,z plane in the same sense as the propeller rotation, i.e. a forward whirl mode.

From equation (A.8) it is seen that in the absence of structural damping and aerodynamic forces the phase angle between the vectors α_1 and β_1 is exactly 90 deg in both whirl modes. When structural damping in the engine freedoms and the aerodynamic excitation from the propellers are taken into account the phase angle differs slightly from 90 deg. The ratios between the vector amplitudes are not quite equal to unity in either mode, the reason being that the engine mount stiffness in the pitching plane is slightly greater than that in the yaw plane, ($K_\alpha/K_\beta = 1.02$).

The frequencies and amplitude ratios of the two whirl modes obtained from numerical solution of the binary flutter equations with $v = 0$ are in close agreement with the theoretical values calculated from equations (A.7) and (A.10) of Appendix A, thus affording a check on the functioning and accuracy of the computer flutter programme.

From Fig. 3 it appears that the frequencies of both whirl modes decrease slightly with increasing airspeed and show only a small dependence on the advance ratio J .

The stability of the whirl motion may be deduced from the curves of decay rate against airspeed. The forward whirl motion, mode 2, becomes increasingly stable as the airspeed rises, with the decay rate at any given airspeed decreasing with increasing J . The backward whirl mode, on the other hand, becomes unstable above a certain critical airspeed, when the decay rate becomes negative. The critical whirl airspeed shows a fairly marked dependence on J , the lowest value of $v_{crit} = 0.25$ being obtained with $J = 2$.

Although J is treated here as an independent variable it is actually a function of propeller r.p.m. and airspeed. For a fixed r.p.m. J is in fact directly proportional to v . The true variation of decay rate with v at maximum take-off propeller r.p.m. is given by the dashed curves labelled $J = 4.24 v$ in Fig. 3. These curves are derived by interpolation between the curves for $J = 1, 2$ and 3.

Both whirl modes remain practically unchanged in form, as determined by the phase angles and amplitude ratios between the vectors, over the whole airspeed range covered, even though the decay rate varies considerably. This behaviour may be contrasted with that of 'classical' flutter, in which two or more basic modes combine to produce a flutter mode of a new form.

4.2. Whirl of the Nacelle in Two Degrees of Freedom.

A binary analysis similar to that described in Section 4.1 was carried out in the vertical and horizontal translational freedoms of the outboard nacelle alone, the engine being considered as rigidly fixed to the nacelle. Structural damping was assumed to be absent from the nacelle freedoms.

The frequencies and decay rates of the two resulting modes are shown in Fig. 4 as functions of dimensionless airspeed v , together with the vector diagrams obtained with $v = 0$. With the sign convention used mode 1 is seen to be a backward whirl motion, while mode 2 is a forward whirl motion. The motion of the propeller hub in each mode is a highly elliptical orbit, unlike the modes derived from the engine freedoms only in which the hub orbit is practically circular. The reason for this is that the bending stiffness of the nacelle in the vertical (x, z) plane is considerably greater than that in the horizontal (x, y) plane, ($K_z/K_y = 1.45$). In the backward whirl mode the major axis of the hub orbit lies parallel to the y -axis, while in the forward whirl mode it lies parallel to the z -axis.

The whirl mode frequencies lie closer together than those derived from the engine freedoms, but similarly decrease only slightly with rising airspeed, and are virtually independent of the advance ratio J .

The decay rate in the forward whirl mode increases with airspeed and decreases with increasing J . The curves of decay rate for the backward whirl mode are very flat, and in the absence of structural damping the mode becomes unstable at $v = 0.35$ for $J = 2$. From the shape of the curves it appears that the backward whirl mode in the nacelle freedoms could be stabilized over a wide range of airspeed by the addition of a relatively small amount of structural damping.

4.3. Whirl of the Complete Engine-Nacelle Installation in Four Degrees of Freedom.

The complete outboard installation, consisting of the engine mounted in gimbals at the end of a flexible cantilever nacelle, was analysed in four degrees of freedom. As described in Section 2.2, motion of the nacelle in parabolic modes in the y and z directions gives rise to yawing and pitching rotations of the gimbal mountings which introduces inertia and aerodynamic coupling between the engine and nacelle freedoms. The damping matrix also contains cross-terms arising from the engine gyroscopic effects; the stiffness matrix on the other hand is diagonal in form, with no coupling. 2 per cent of critical structural damping was assumed to act in the engine freedoms only.

Details of the four modes of vibration calculated for $v = 0$ and $J = 2$ are given in Fig. 6, which shows the amplitude ratios and phase relationships between the vectors associated with each of the four degrees of freedom considered. Also shown are the loci of the propeller hub and gimbal point in their respective y, z planes in each mode. Numbered points on each locus denote successive positions of the hub and gimbal when viewed from ahead, starting from an arbitrary origin.

The y and z co-ordinates of the gimbal point and propeller hub are related to the generalised co-ordinates by the following equations: (see Fig. 2). For the gimbal point G :

$$y_G = y_1$$

$$z_G = z_1$$

for the propeller hub P :

$$y_P = (1 + r_\psi l_p) y_1 + l_p \beta_1$$

$$z_P = (1 + r_\theta l_p) z_1 - l_p \alpha_1.$$

It should be noted that each vector diagram in Fig. 6 is drawn to an arbitrary amplitude scale, consequently the mode shapes derived from them are all to different amplitude scales. The four modes are numbered in ascending order of frequency and are described below.

Mode 1. In mode 1 vector y_1 leads vector z_1 by nearly 90 deg, which indicates a backward whirl motion of the gimbal point G at the end of the nacelle (compare with vector diagram of Fig. 4). Superimposed on this motion is a backward whirl in the engine freedoms, with vector α_1 leading vector β_1 by nearly 90 deg. The phase angles between y_1 and z_1 and between α_1 and β_1 differ from 90 deg because of the presence of 2 per cent critical structural damping in the engine freedoms. The effect of this is to rotate the major and minor axes of the elliptical orbits traced by G and P slightly away from the y and z axes.

The phase relationship between the nacelle whirl and engine whirl motions is such that the rotations of the engine relative to the gimbal tend to augment the amplitude of the propeller motion arising from the translations of the gimbal and the slopes at the nacelle tip. The total motion of P relative to the x -axis is thus a backward whirl, of large amplitude. These engine and nacelle whirl motions may be regarded as being 'in-phase'.

Mode 2. In mode 2 vector y_1 lags vector z_1 by nearly 90 deg, giving the gimbal a highly elliptical forward whirl motion (compare with Fig. 4). Vector α_1 leads β_1 by nearly 90 deg, which denotes a backward whirl motion of the engine relative to the tangent to the nacelle at point G . However the engine rotations are of such small relative amplitude that the total motion of the propeller hub P is a forward whirl dominated by the nacelle freedoms.

Mode 3. In this mode a backward whirl motion of the engine is superimposed on a backward whirl of the nacelle. Unlike mode 1, however, the phase relationship between the vectors is such that the rotations of the engine relative to the nacelle oppose the displacements and rotations of the nacelle tip so as to reduce the total displacements of the propeller hub. These engine and nacelle whirl motions may be regarded as 'out of phase'.

Mode 4. This is a forward engine whirl superimposed on a forward nacelle whirl, with the engine rotations again opposing the nacelle displacements. In this case the engine rotations are sufficiently large actually to reverse the sign of the total displacements of the propeller hub P , causing it to lead the gimbal point G by approximately 180 deg.

The behaviour of the modes with increasing airspeed is illustrated in Fig. 5, which shows the frequencies and damping rates as functions of v for values of $J = 1, 2$ and 3 .

The frequencies of modes 1 and 4 decrease very slightly as v increases, while those of modes 2 and 3 remain nearly constant. All frequencies show a very slight decrease with increasing J , this effect being more marked at the higher airspeeds.

Modes 2 and 4 are stable, and become increasingly stable with rising airspeed. In each of these modes both the gimbal and propeller hub exhibit forward whirl motion. The decay rate at $v = 0$ in mode 2 is slight, due to the small part played by the engine freedoms, which contain the only structural damping present in the system. The decay rate decreases with increasing J at moderate airspeed.

Mode 3, in which both gimbal and propeller hub exhibit backward whirl motion, is stable over the whole range of airspeed investigated, though the increase in stability with airspeed is not so pronounced as in modes 2 and 4.

Mode 1 on the other hand becomes unstable as airspeed increases, with the decay rate becoming zero at a critical value of $v = 0.20$, with $J = 2$.

From these results and those of the previous two sections the following conclusions may be drawn as to the stability of whirl motion.

(i) In two degrees of freedom, either those of the engine or of the nacelle, the forward whirl motion appears to be inherently stable, while the backward whirl motion becomes unstable above a certain critical airspeed.

(ii) With four degrees of freedom in play those modes in which both the gimbal and the propeller hub exhibit forward whirl motion are stable.

(iii) The stability of modes in four degrees of freedom in which both the gimbal and propeller hub exhibit backward whirl motion depends on the phase relationship between the engine and the nacelle motions. If this is such as to produce large amplitude displacements of the propeller (e.g. mode 1) the mode may become unstable with increasing airspeed owing to the large excitation provided by the aerodynamic forces and moments acting on the propeller. On the other hand, if, the phase relationship is such that the amplitude of the propeller motion is small, the aerodynamic excitation may not be great enough to overcome the structural damping and stiffness of the system, and the motion will remain stable.

(iv) The form of the whirl modes and their frequencies show very little change with airspeed, right up to and beyond the critical airspeed.

4.4. Whirl in Four Degrees of Freedom with Gyroscopic Effects Neglected.

The analysis in four degrees of freedom described in Section 4.3 was repeated with the terms arising from the engine gyroscopic moments omitted from the flutter matrices, and with no structural damping. The aerodynamic forces and moments acting on the propeller were evaluated as before for $J = 2$. The frequencies and decay rates of the resulting modes are shown in Fig. 7, together with schematic representations of the mode shapes at zero airspeed.

At $v = 0$ the modes 2 and 4 arise from inertia coupling between the freedoms z_1 and α_1 in the x,z plane. In mode 2 vector z_1 leads vector α_1 by exactly 180 deg, giving rise to large displacements of the propeller, while in mode 4 z_1 and α_1 are in phase, with a correspondingly small propeller amplitude. In a similar manner modes 1 and 3 result from inertia coupling between the freedoms y_1 and β_1 in the x,y plane, with mode 1 having the large propeller amplitude. In the absence of gyroscopic terms no coupling exists at zero airspeed between the vertical and horizontal freedoms.

As the airspeed is raised aerodynamic forces acting on the propeller provide this coupling, until at $v \approx 0.50$ the frequencies of modes 1 and 2 tend to approach each other and two new modes emerge, similar in form to the whirl modes of Section 4.3. One of these modes, the forward whirl mode, becomes very stable, while the backward whirl mode becomes unstable at $v = 0.48$.

It therefore appears that an unstable whirl motion may be brought about solely by aerodynamic forces and moments acting on the propeller in the 'classical' flutter manner, with two basic modes combining to produce a new and unstable flutter mode.

On the other hand, although gyroscopic moments can provide the coupling necessary to produce whirl motions, even in the absence of aerodynamic forces, it is shown in Appendix A that these are always neutrally stable. Gyroscopic moments acting alone cannot lead to instability as they do not feed energy into the system; they do however exercise a considerable influence on the frequencies and forms of the whirl modes.

4.5. The Effect of Engine Mount and Nacelle Stiffnesses on the Whirl-mode Shapes and Frequencies.

Flutter analyses in four degrees of freedom were carried out on the outboard engine-nacelle installation over a range of engine mount and nacelle stiffnesses. Aerodynamic and gyroscopic forces and moments were evaluated as before at maximum engine take-off r.p.m. at sea level for an advance ratio of $J = 2$. 6 per cent of critical structural damping was assumed for the engine freedoms, the nacelle freedoms were considered to be undamped.

The independent variables chosen were the uncoupled natural frequency of the engine pitching freedom

(ω_α) and the uncoupled frequency of the nacelle vertical freedom (ω_z). For convenience it was assumed that $\omega_\beta = \omega_\alpha$ and $\omega_y = \omega_z$. It should be noted that each of the uncoupled natural frequencies is proportional to the square root of the direct stiffness in the associated degree of freedom.

The zero airspeed frequencies of the four modes are shown in Fig. 8 as functions of ω_α , for three values of ω_z . The frequencies are all reduced to a non-dimensional form by dividing by the parameter $\Omega_1 = \Omega I_p (I_\theta I_\psi)^{-\frac{1}{2}}$. As shown in Appendix A, this is a useful parameter in the frequency equations since it incorporates the effects of the propeller r.p.m. and of the engine inertias. For comparison the theoretical values of the forward and backward whirl frequencies of a binary system in the engine freedoms are also plotted on Fig. 8, together with the theoretical nacelle binary whirl mode frequencies which form the asymptotic limits to the quaternary whirl frequencies as ω_α tends to infinity. These theoretical frequencies are derived from equation (A.17), with $\Omega_1 = 5.84$ cycles/second.

The zero airspeed frequency of mode 1 is shown in Fig. 9 as a function of ω_α and ω_z , a carpet plot being used to facilitate interpolation. The asymptotic limits set by the theoretical frequencies of the backward binary engine and nacelle whirl motions are included.

The vector diagrams associated with the four whirl modes at zero airspeed are shown in Fig. 10 for four combinations of ω_α and ω_z . The decay rates of the four whirl modes are shown as functions of the dimensionless airspeed v in Fig. 11 for each combination of ω_α and ω_z .

With a relatively stiff nacelle and flexible engine mounts (e.g. case (a) of Fig. 10), the engine freedoms dominate modes 1 and 2, while the nacelle freedoms dominate modes 3 and 4.

In modes 1 and 3 a backward whirl of the engine about the gimbals is superimposed on a backward whirl of the nacelle. In mode 1 these constituent whirl motions are ‘in phase’, while in mode 3 they are ‘out of phase’ (see Section 4.3). In modes 2 and 4 both engine and nacelle exhibit forward whirl motions; in mode 2 they are in phase, while in mode 4 they are out of phase.

From the frequency plots of Fig. 8c it is seen that with the engine freedoms playing the dominant role at low values of ω_α , the frequencies of modes 1 and 2 lie close to the theoretical backward and forward whirl frequencies respectively of a binary system in the engine freedoms alone. Similarly, with the nacelle freedoms dominating modes 3 and 4 their frequencies approximate to the theoretical nacelle binary-whirl frequencies.

If the engine mount stiffnesses (i.e. ω_α and ω_β) are increased, with the nacelle stiffnesses remaining unchanged, the nacelle freedoms play increasingly large parts in modes 1 and 2 (Fig. 10, case (b)). Their frequencies approach the limits set by the theoretical nacelle binary backward and forward whirl frequencies respectively, (Fig. 8c). Modes 3 and 4 on the other hand show very little change, their frequencies rising slightly with increasing ω_α . It should be noted that the directions of the component engine and nacelle whirl motions in all four modes, and also the phase relationships between them, remain unchanged over the whole range of ω_α considered, for this particular value of ω_z .

If the nacelle stiffnesses are decreased (Fig. 10 case (c)) the nacelle freedoms play a much greater part in mode 1 and completely dominate mode 2. Mode 1 retains the character of a backward engine whirl in phase with a backward nacelle whirl. Mode 2, however, shows unexpected behaviour in that while the nacelle whirl remains forward the engine whirl component reverses its direction and becomes backward. Mode 3 remains virtually unchanged, while the engine freedoms play a larger part in mode 4. At low values of ω_α the frequency of mode 1 lies close to the engine binary backward whirl frequency. The frequency of mode 2 lies just below the limit set by the nacelle binary forward whirl frequency, (Fig. 8a). The closeness of the separate engine and nacelle binary whirl frequency limits for this particular combination of ω_α and ω_z probably accounts for the unusual behaviour of mode 2. As ω_α is increased modes 1 and 2 both become dominated by the nacelle freedoms and their frequencies approach those of the nacelle binaries. Modes 3 and 4 remain practically unchanged in form, their frequencies increasing almost linearly with ω_α .

From Fig. 9 it appears that the zero airspeed frequency of mode 1 is always less than the lower of the two backward binary-whirl frequencies in the engine or nacelle freedoms alone. Each of these binary-whirl frequencies forms an asymptotic limit to the frequency of the quaternary mode 1 as the stiffness in the other pair of freedoms becomes infinitely great.

The variation with airspeed of the decay rates of the four whirl modes is illustrated in Fig. 11, in which the decay rates ζ_r (equation (5b)) for each of the modes are plotted against dimensionless airspeed v .

Those modes in which the engine freedoms play only a small part decay slowly at zero airspeed; this is because no structural damping was included in the nacelle freedoms. Of the four modes only the low frequency backward whirl mode (mode 1 in all cases) becomes unstable over the airspeed range covered. This mode is composed of the backward nacelle and engine binary whirl motions in phase. Mode 3, which is the out of phase combination of the backward binary whirl motions, shows a slight falling off in decay rate with rising airspeed in case (d). This mode does, however, remain stable over the range covered, and a spot check at $v = 2.0$ showed a levelling out in the slope of the decay rate curve, with the mode remaining stable. The two forward whirl modes 2 and 4 show a marked rise in stability with increasing airspeed in all cases.

The frequencies of modes 2, 3 and 4 show very little change over the whole range of airspeed covered. The shapes of the modes, as indicated by the relative amplitudes and phase angles of the vectors, remain virtually unchanged over the airspeed range. This is also true of mode 1, for which the frequency and vector diagram shows little change up to and beyond the airspeed at which the mode becomes unstable.

It appears that the frequencies and shapes of the whirl modes are determined by the characteristics of the installation, such as mount stiffness and propeller r.p.m., rather than by airspeed. Whirl motion of an engine installation thus differs from the classical flutter instability, in which aerodynamic forces provide coupling between normal modes of a structure to give rise to a new flutter mode above a critical value of the airspeed.

Since it is the behaviour of mode 1 that determines the stability of the engine-nacelle installation, attention will now be concentrated on the critical value of airspeed at which this mode becomes unstable, and the manner in which this critical value is influenced by other parameters.

4.6. *The Effects of Engine-mount Stiffness and Damping on the Critical Whirl Airspeed.*

The critical whirl airspeed v_{crit} is here taken to be the value of dimensionless airspeed above which mode 1 becomes unstable, i.e. its decay rate becomes negative.

The effects of engine mount and nacelle stiffnesses on v_{crit} are shown in Fig. 12, in which v_{crit} is plotted as a function of ω_α and ω_z . Structural damping equal to 6 per cent of the critical value was introduced into the engine freedoms, and none into the nacelle freedoms. As before, propeller aerodynamic and gyroscopic forces were evaluated at maximum r.p.m. at sea level and with $J = 2$.

As shown in Section 4.5, if a relatively flexible engine-mount system is combined with a stiff nacelle structure the engine freedoms dominate mode 1. Under these conditions v_{crit} tends towards the value obtained for a binary system in the engine freedoms alone. Thus with low values of ω_α little increase in v_{crit} is gained from a large increase in ω_z . Conversely, if the nacelle is lowly damped and very flexible (ω_z low), little gain in v_{crit} is to be had from an increase in engine-mount stiffness, (Fig. 12).

The effect on v_{crit} of damping in the engine mounting is shown in Fig. 13, in which v_{crit} is plotted as a function of ω_α and ζ_α for a fixed value of $\omega_z/2\pi = 4.78$ cycles/second. This corresponds to a relatively flexible nacelle with no structural damping. v_{crit} is always raised by an increase in engine-mount damping coefficient ζ_α , and may also be raised up to a certain limit by increasing ω_α . The damping in the whirl mode arising from the structural damping in the engine mount is lost if ω_α is increased to such an extent that the mode becomes dominated by the nacelle freedoms. Under these conditions v_{crit} may actually decrease as the engine-mount stiffness is raised. Eventually, as ω_α is increased still further, v_{crit} tends to the value obtained for a binary in the nacelle freedoms only, which is naturally independent of ζ_α .

5. *The Whirling Motion of a Nacelle-Engine Installation Mounted on a Flexible Wing.*

In order to investigate the influence of wing flexibility on the whirling of an engine installation, and also the effect of engine whirl on the stability of the wing itself, further flutter analyses were carried out in twelve degrees of freedom. Four freedoms were assigned to the wing and four to each of two engine installations similar to that considered in Section 4.

Mass and stiffness data for the two installations are given in Table 1. The outboard installation is

identical to that of Section 4.3, while the inboard installation has approximately 40 per cent greater nacelle stiffnesses.

The wing freedoms chosen are four of the antisymmetric normal modes of the wing of a typical modern turbo-prop aircraft. These were derived from calculations based on arbitrary branch modes, and include the effects of flexible nacelles and engine mountings with freedom in the vertical planes only, but exclude terms arising from propeller aerodynamic and gyroscopic effects. These four normal modes of the wing are illustrated in Fig. 14 and are described below in terms of their component branch modes. For this purpose the wing is divided into three regions, namely, inner wing (root to inboard engine), mid-wing (inboard engine to outboard engine) and outer wing (outboard engine to tip). The bending and twisting deflections of each section, forming the branch modes of the original analysis, are measured relative to the end of the adjacent section on the inboard side.

Freedom 1.

Positive fuselage roll (anticlockwise viewed from ahead); positive fundamental bending of inner, mid and outer wing; positive torsion (nose up) of inner and mid wing.

Freedom 2.

Negative fuselage roll; positive fundamental bending of inner, mid and outer wing; positive torsion of inner wing and negative torsion of mid-wing.

Freedom 3.

Negative fuselage roll; positive fundamental bending of inner, mid and outer wing; negative torsion of inner wing.

Freedom 4.

Negative bending of mid wing, positive bending of outer wing; slight positive torsion of inner and mid wing, high degree of positive torsion of outer wing.

5.1. Flutter of the Wing with Rigid Engine Installations.

A flutter analysis was performed in the four undamped wing freedoms with the engine and nacelle freedoms suppressed, i.e. the installations considered to be infinitely stiff. The frequencies and decay rates of the four resulting modes are shown in Fig. 15 as functions of airspeed. Also shown are the mode vectors at zero airspeed.

The damping in all four modes (arising from the wing aerodynamics only) increases up to $v = 0.5$, beyond which the stability of modes 2 and 4 shows a sharp drop. By $v = 0.685$ a new and unstable mode has appeared, composed mainly of freedoms 3, 2 and 1. This new mode can also be regarded as the result of coupling between modes 1 and 2, whose frequencies approach each other at about $v = 0.68$. Another new mode appears in this range of airspeed, consisting mainly of freedoms 4, 2 and 3, with a small contribution from 1, and becomes unstable at $v = 0.72$. From the vector diagrams this new mode appears to be a combination of modes 2 and 4.

5.2. Flutter of the Wing plus Flexible Engine Installations, with Propeller Aerodynamic and Gyroscopic Effects Neglected.

The results of a flutter analysis in all twelve degrees of freedom of the wing and two engine installations are presented in Figs. 16 and 17. The aerodynamic and gyroscopic forces arising from the propellers and engines were omitted from the flutter matrices, the only excitation coming from aerodynamic forces acting on the wing itself. No structural damping was included. The modes derived from the analysis are numbered in ascending order of frequency at zero airspeed.

Modes 4 and 9 consist of horizontal translation of the inboard nacelle coupled with yawing of the inboard engine. Modes 2 and 8 are similar modes of the outboard installation. In the absence of propeller and gyroscopic effects these modes are not coupled with the others, and remain undamped and constant in frequency over the airspeed range.

Of the other modes only modes 1, 3 and 7 become unstable within the airspeed range covered. The

vector diagrams for these three modes are presented in Fig. 17 for $v = 0$, and also for those values of v at which each mode becomes unstable. For clarity the vectors for the wing and the two engine installations are shown separately; for interpretation of relative amplitudes and phase angles they should be regarded as having a common origin.

Mode 1. At $v = 0$ this mode consists mainly of wing freedoms 1 and 3 plus vertical translation and pitching of the outboard nacelle and engine (freedoms 9 and 10). In effect this is similar to mode 1 of Fig. 15, plus a contribution from the outboard installation. At $v = 0.73$ the mode becomes unstable and also changes its character, with wing freedoms 2 and 3 coming into play and with a phase change of about 165 deg in the inboard installation motion. In addition the frequency shows an increase of 18 per cent over the value at $v = 0$. Under these conditions (i.e. flutter) the mode appears to be similar to mode 2 of Fig. 15, with the addition of the outboard installation motions.

Mode 3. At $v = 0$ this mode consists mainly of wing freedoms 2 and 3 (compare with mode 3 of Fig. 15), coupled with vertical freedoms of the inboard installation, with a smaller contribution from the outboard installation. The mode becomes unstable at $v = 0.86$, with a slight change in character arising from an increase in the contribution from wing freedom 3 and a phase advance of 195 deg in the motion of the outboard installation.

Mode 7. At $v = 0$ this consists of wing freedom 3, plus small contributions from both engine installations. The mode becomes unstable at $v = 0.74$ without appreciable change in character apart from the phase shifts in the low amplitude motions of the engine installations.

5.3. *Flutter of Wing plus Flexible Engine Installations, with Propeller Aerodynamic and Gyroscopic Effects Included.*

The full twelve degree of freedom system was re-analysed with the propeller aerodynamic and gyroscopic terms included in the flutter matrices. These were evaluated as before, at maximum propeller r.p.m. at sea level and with $J = 2$. Viscous damping (2 per cent of critical) was introduced into the pitching and yawing freedoms of both engines relative to their nacelles. The resulting modes are presented in Figs. 18 and 19. The three modes which become unstable in the airspeed range are described below.

Mode 1. At $v = 0$ this is composed of wing freedoms 1 and 3 (compare mode 1 of Fig. 17) coupled with a large scale backward whirl motion of the outboard engine installation and a small scale backward whirl of the inboard installation. The backward whirl of the outboard installation is practically identical with that of the same installation mounted on a rigid structure (compare with mode 1 of Fig. 6), and the frequency of the mode is only slightly less than that of mode 1 of Fig. 6. The mode becomes unstable at $v = 0.22$, with no change in the power-plant whirl motions and only a slight drop in frequency. When mounted on a rigid structure the outboard installation backward whirl mode becomes unstable at $v = 0.20$ (Section 4.3).

Mode 2. This consists mainly of a backward whirl of the inboard power plant coupled with wing freedoms 3, 2 and 1. The mode becomes unstable at $v = 0.23$ with virtually no change in character apart from a phase lag of about 75 deg in freedom 1.

Mode 5. At $v = 0$ this consists mainly of an out of phase combination of a backward whirl of the outer nacelle and a backward whirl of the outer engine, somewhat similar to the mode 3 described in Section 4.3 (see Fig. 6). This is coupled with a small amplitude forward whirl of the inboard nacelle (freedoms 5 and 7), and also with a small contribution from wing freedoms 3 and 2. The mode becomes unstable at $v = 0.82$, when the wing freedoms 3, 2 and 4 combine to produce a mode similar to mode 7 of Fig. 17. The whirl motion of the outboard installation continues with little change. The inboard installation exhibits a distorted form of whirl motion with highly elliptic orbits inclined to the y and z axes.

Of the other modes of Fig. 18, modes 11 and 12 are similar to modes 11 and 12 of Fig. 16. Since their frequencies are well above any of the whirl frequencies of the power plants they are unaffected by the propeller aerodynamic and gyroscopic forces. Mode 10 may be identified with the forward whirl motion of the outboard power plant installation (mode 4 of Fig. 6), and mode 9 with the corresponding motion

of the inboard installation. With their frequencies lying outside the main frequency spectrum of Fig. 16 they appear to be unaffected by the wing motions. The remaining modes, 3, 4, 6, 7 and 8 are all formed by coupling between the modes of Fig. 16 and the intermediate frequency whirl modes of the power plants, i.e. those similar to modes 2 and 3 of Fig. 6. None of these modes become unstable within the airspeed range.

From all these results it appears that wing flexibility has no appreciable effect on a whirl motion of either power plant whose frequency lies outside the frequency spectrum of the modes obtained in the absence of propeller aerodynamic and gyroscopic forces. On the other hand an unstable flutter motion of the wing may be stabilised up to a higher flutter speed by a stable power-plant whirl motion of comparable frequency. The results, however, give no indication of the effects of interaction between an unstable wing-flutter mode and an unstable power-plant whirl mode of comparable frequency.

5.4. *The Effect of Frequency Coincidence between Wing Modes and Power-plant Whirl Modes.*

The conclusions drawn in the previous section may only hold in cases where the frequencies of the critical whirl modes of the power plants are well removed from those of the wing modes. With stiffer nacelles and engine mounts than those previously considered the possibility arises of frequency coincidences and coupling between the power-plant whirl modes and one or more of the wing modes, which may have a destabilizing effect on a whirl mode or even precipitate wing flutter.

In order to investigate this possibility the twelve degrees of freedom system considered in Section 5.3 was re-analysed with the structural stiffnesses of the outer nacelle and engine mounts increased by a factor of four, which has the effect of doubling the uncoupled natural frequencies ω_x , ω_z etc. From the results of Section 4.5 this would be expected to raise the frequency of the unstable backward whirl mode from 2 cycles/second to around 5.5 cycles/second, thus bringing it within the band of wing mode frequencies. The inboard installation was left unchanged.

As a check the stiffened outboard nacelle-engine installation was itself analysed in four degrees of freedom. The frequencies, vectors, and damping rates for these four whirl modes are shown in Fig. 20. The new backward whirl mode 1 has a zero airspeed frequency of 5.45 cycles/second and becomes unstable at $v = 0.48$.

The results of the analysis in all twelve degrees of freedom are presented in Figs. 21 and 22. Four modes become unstable in the airspeed range covered and these are described below; their vector diagrams are shown in Fig. 23.

Mode 1. This is almost identical with mode 2 of Fig. 19, obtained with the original outboard installation, and consists mainly of a backward whirl motion of the inboard nacelle and engine, which becomes unstable at $v = 0.23$ as before. Changes in the outboard installation have no effect on this mode.

Mode 2. At $v = 0$ this consists mainly of wing freedoms 1 and 3, coupled with a backward whirl of the inboard and outboard nacelles. At about $v = 0.55$ the mode undergoes a complete change in character and shows a drop in decay rate leading to instability at $v = 0.66$ (Fig. 22). This appears to be brought about by a frequency coincidence and coupling with mode 3. The situation is comparable with that occurring in Fig. 18 between modes 3 and 4 (which correspond to modes 2 and 3 of the present case), in which mode 4 shows a sharp drop in decay rate, without however actually becoming unstable. The outboard installation continues in its backward whirl motion while the motion of the inboard installation becomes heavily distorted. The instability of the mode 2 thus appears to be primarily a wing flutter, aggravated but not precipitated by whirl of the power plant installations.

Mode 4. At $v = 0$ this comprises a backward whirl of the outboard installation, comparable with mode 1 of Fig. 20, plus a forward whirl of the inboard installation and also contributions from wing freedoms 3, 4 and 2.

At $v = 0.92$ the mode becomes unstable, with wing freedoms 1 and 2 becoming prominent. This change in mode shape probably results from a frequency approach and consequent coupling between modes 4 and 3 (see Fig. 21). At the same time the backward whirl of the outboard installation grows in amplitude and may itself become unstable. When mounted on a rigid structure, however, it becomes unstable at $v = 0.48$ (see Fig. 20).

Mode 8. At $v = 0$ this consists of wing freedoms 1, 4 and 3, with a forward whirl of the inboard installation and a stable whirl of the outboard installation (compare with mode 2 of Fig. 20). As v increases the mode changes shape, with wing freedoms 3 and 4 playing larger parts and the amplitude of the engine installation whirl motions increasing, until instability occurs at $v = 0.75$.

The large drop in frequency of mode 8 with rising airspeed suggests that the instability of the mode is a true flutter behaviour brought about by a coupling with another mode. Mode 6 appears to be the likely partner in this case, since it shows a rise in frequency towards that of mode 8 and also a sharp increase in stability after mode 8 has become unstable.

From these results it appears that, if the frequency of a normally unstable backward whirl mode of an installation lies within the frequency band of the wing modes, then the whirl mode may be stabilised by the wing motion. On the other hand the behaviour of mode 2 suggests that the stability of a wing flutter mode may be reduced by an approaching frequency coincidence with a critical backward whirl mode.

6. Conclusions.

6.1. *The Nature of Whirling Motion.*

(1) A typical installation consisting of a turbo-prop engine supported at the end of a long nacelle cantilevered from an aircraft wing may in certain circumstances exhibit a precessional type of motion commonly referred to as 'whirling'. In this motion, which should not be confused with the whirling instability of rotating flexible shafts, the engine and propeller hub describe elliptical orbits in a plane perpendicular to the propeller shaft axis, at frequencies differing from the propeller rotational frequency. Two types of whirl motion have been observed, a forward precession in the same direction as the propeller rotation and a backward precession against the direction of the propeller rotation.

(2) Whirl motion results from coupling between pitching and yawing motions of the engine and propeller. Such coupling is provided by the gyroscopic moments arising from the rotating engine and propeller masses and by aerodynamic forces and moments acting on the propeller at incidence to the airstream.

(3) Pitching and yawing motions of the engine can be considered as arising in two ways, either from pure rotations of the engine about an effective gimbal mounting or, as in the case of an engine rigidly attached to a nacelle structure, from the slopes at the tip of the nacelle resulting from its deflections as a cantilever. For simplicity the complete engine-nacelle installation may be analysed as a binary system in either the two engine freedoms or the two nacelle freedoms. In a typical installation, however, the engine and nacelle freedoms are coupled through inertia and aerodynamic effects and it is generally necessary to analyse it as a quaternary system in all four degrees of freedom simultaneously.

6.2. *Whirling Motion of an Engine Installation in Two Degrees of Freedom.*

(1) It is shown in Appendix A that, in the absence of aerodynamic forces, the equations of motion for the binary systems in either the engine or nacelle freedoms are of a similar form when expressed in terms of suitable parameters. The two systems may therefore be regarded as equivalent.

(2) The zero-airspeed frequencies of the binary whirl modes in either the engine or nacelle freedoms, as obtained from numerical solution of the flutter equations, are in close agreement with the theoretical values derived in Appendix A.

(3) The zero-airspeed frequency of the forward whirl mode is always greater than the higher of the two uncoupled natural frequencies of the system, and increases with rising propeller r.p.m. The frequency of the backward whirl mode is always less than the lower of the uncoupled natural frequencies and decreases with rising propeller r.p.m. The frequencies of both modes decrease slightly with increasing airspeed but are virtually independent of the advance ratio J .

(4) The damping in the whirl modes arises only from structural damping inherent in the system, e.g. direct damping at the gimbal mounts, and from aerodynamic forces acting on the propeller at incidence to the airstream. The engine gyroscopic torques do not themselves contribute to the damping in the whirl modes (see Appendix A).

(5) The stability of the whirl modes may be judged from the curves of decay rate against airspeed. The forward whirl modes in either the engine or nacelle freedoms appear to be inherently stable, with the stability increasing steadily as the airspeed rises. In the backward whirl modes, however, the stability at first increases and then decreases with rising airspeed, until above a critical value of airspeed the decay rate becomes negative and the motion unstable.

6.3. Whirling Motion of an Engine Installation in Four Degrees of Freedom.

(1) The modes obtained in the quaternary system may be regarded as combinations of the two pairs of binary modes from the engine and nacelle freedoms. Two forward whirl modes and two backward whirl modes may be identified. In one of the forward and one of the backward modes the nacelle and engine freedom vectors are in phase, resulting in relatively large displacements of the propeller hub. In the other pair of modes the nacelle and engine-freedom vectors are very nearly 180 deg out of phase, producing small propeller displacements.

(2) The frequency of the quaternary 'in-phase' forward whirl mode is always less than the lower of the two binary forward mode frequencies obtained by suppressing the cross-coupling between the engine and nacelle freedoms. Each of the binary forward whirl mode frequencies becomes the asymptote to the quaternary 'in-phase' forward whirl mode frequency as the other binary forward mode frequency becomes relatively great. A similar relationship holds between the frequencies of the 'in-phase' quaternary backward whirl mode and the binary backward whirl modes.

(3) The frequency of the 'out-of-phase' forward quaternary whirl mode is higher than the greater of the two binary forward whirl modes, and similarly for the 'out-of-phase' backward quaternary mode and the backward binary modes. Thus the theoretical binary mode frequencies as calculated from the equations given in Appendix A serve as useful bounding values for the quaternary mode frequencies.

(4) Both the forward quaternary whirl modes are stable over the airspeed range covered. The 'out-of-phase' backward whirl appears to be stable over the airspeed range covered, though with certain combinations of engine mount and nacelle stiffnesses the stability in this mode shows a slight drop as the airspeed increases. The 'in-phase' backward whirl mode becomes unstable at a critical airspeed which may be below the critical value for either of the two binary backward whirl modes.

(5) The critical value of airspeed at which the 'in-phase' backward whirl mode becomes unstable depends largely on the amount of structural damping present and on the stiffness of the nacelle and engine mounts. The critical whirl airspeed may be raised considerably by introducing damping into the engine mounts. A similar result could probably be obtained by introducing structural damping into the nacelle structure, although as this is much more difficult to achieve in practice its effect was not investigated here.

The critical whirl airspeed may be raised by increasing the stiffnesses in either the engine or the nacelle freedoms, although the effect of this is slight if the stiffnesses in the other pair of freedoms are relatively low. Under certain conditions, e.g. a heavily-damped engine mounting in combination with a flexible, lightly-damped nacelle structure, an increase in the engine-mount stiffness beyond a certain point may lead to a drop in the critical whirl airspeed.

6.4. The Interaction between Wing-flutter Modes and Power-plant Whirl Modes.

From the results obtained from a system consisting of a flexible wing with four degrees of freedom plus two engine-nacelle installations, the following tentative conclusions may be drawn as to the effect of wing flexibility on the whirl of the engine installations.

(1) If the frequency of the critical backward whirl mode of an installation lies well below the band of wing mode frequencies at zero propeller r.p.m., then the mode shape, frequency and stability of the whirl motion are unaffected by the wing motions.

(2) If the frequency of the critical backward whirl mode lies within the band of wing frequencies, the whirl mode may be stabilized up to a higher critical airspeed.

(3) A stable whirl mode of an installation, e.g. a forward whirl mode or the out-of-phase backward whirl mode, does not appear to be destabilised by wing motion, even in a wing mode of comparable frequency.

Since in no case is the stability of a power-plant whirl mode adversely affected by motion of the wing, the analysis of power-plant whirl may in general be limited to the four degrees of freedom of the installation itself with the wing being considered rigid, although this may lead to a pessimistic result. As to the influence of power-plant whirl motion on the flutter of the wing itself, it appears that a wing-flutter mode may be stabilized up to a higher flutter speed by coupling with a stable whirl mode of comparable frequency. On the other hand the stability of a wing flutter mode may be reduced by coupling with an unstable power-plant whirl mode of comparable frequency, leading to a decrease in the flutter speed.

It should be borne in mind that the above tentative conclusions have been drawn from the results of a strictly limited range of cases calculated for a system with only four degrees of freedom allowed to the wing. Because of the many variables involved, and of the difficulties of interpreting the results of flutter calculations in many degrees of freedom, it is not practicable to cover a range of conditions wide enough to enable general conclusions to be drawn as to the effects of power-plant whirl motion on wing flutter. It is therefore advisable when investigating wing flutter to include the power-plant pitching and yawing freedoms, with their associated gyroscopic and propeller aerodynamic terms, in the original analysis.

LIST OF SYMBOLS

$[A]$	Inertia matrix
$[B]$	Aerodynamic-damping matrix
$[C]$	Aerodynamic-stiffness matrix
$[E]$	Structural-stiffness matrix
a, b, c, e	Scaled forms of the above matrices, as defined in equation (3)
c_m	Reference wing chord (ft)
$C_{y\psi}, C_{z\psi}$, etc	Propeller aerodynamic derivatives in equation (34)
F_z, F_y	Aerodynamic forces acting on the propeller in the z and y directions respectively (lb)
I_θ, I_ψ	Moments of inertia in pitch and yaw respectively of the engine plus propeller, measured about the gimbal mount point (slug/ft ²)
I_P	Polar moment of inertia of propeller and rotating engine parts, referred to the propeller rotational speed (slug/ft ²)
J	Advance ratio $V/2NR$
K_α, K_β	Effective rotational stiffnesses of the engine gimbal mounts in pitch and yaw (lb ft/rad)
K_z, K_y	Effective stiffnesses of nacelle cantilever, referred to displacements in the z and y directions (lb/ft)
l, l_E, l_P	Dimensions of engine/nacelle installation (ft), (see Fig. 1)
M_θ, M_ψ	Aerodynamic moments acting on propeller in pitch and yaw respectively (lb/ft)
$[M_E], [M_N]$	Diagonal matrices of engine and nacelle masses respectively
m_E	Mass of engine plus propeller (slug)
N	Propeller rotational speed (rev/sec)
q_i	i^{th} generalised co-ordinates in Lagrange's equation
Q_i	i^{th} generalised force in Lagrange's equation
r_θ, r_ψ	Ratios of tip slopes to tip deflections of nacelle cantilever in the pitch and yaw planes respectively
R	Propeller radius (ft)
S	Area of propeller disc (ft ²)
$[T_E], [T_{WN}]$, etc	Transformation matrices defined in Section 3
\mathfrak{J}	Kinetic energy (lb ft)
U	Potential energy (lb ft)
V	True airspeed (ft/sec)
V_0	Reference airspeed in flutter equation (ft/sec)
v	Dimensionless airspeed = V/V_0

LIST OF SYMBOLS (contd.)

x, y, z	Orthogonal co-ordinate system (Fig. 1)
x_P, x_E, x_G	Dimensions of engine/nacelle installation (ft)
x_n	Distance of n^{th} concentrated nacelle mass from wing flexural axis (ft)
y_E, z_E	Displacements of engine c.g. (ft)
y_P, z_P	Displacements of propeller
z_W	Displacement of a point on the wing flexural axis (ft)
y_1, z_1	Displacements of gimbal mount point relative to tangents at nacelle root (ft)
α_1, β_1	Rotations of engine relative to nacelle in pitch and yaw respectively (rad)
$[\Delta_w]$	Transformation matrix defined in equation (11)
$\zeta_\omega, \zeta_\beta$	Viscous-damping coefficients in the engine freedoms, expressed as a percentage of the critical damping
ζ_r	Decay rate in the r^{th} mode, defined in equation (5b)
θ, ψ	Angular displacements of propeller relative to airstream in pitch and yaw respectively, (rad)
$\bar{\theta}, \bar{\psi}$	Effective angular displacements of propeller, as defined in equation (35)
λ_r	r^{th} complex root of flutter determinant
μ_r	Real part of λ_r
ρ	Air density (slug/ft ³)
ρ_0	Air density at sea level (slug/ft ³)
σ	Air density ratio = ρ/ρ_0
τ	Dimensionless time = tV_0/c_m
Ω	Propeller rotational speed, (rad/sec)
Ω_1	Reduced propeller rotational speed, defined in equation (A.4) (rad/sec)
Ω_2	Reduced propeller rotational speed, defined in equation (A.14) (rad/sec)
ω_p	Total angular velocity of propeller about the displaced shaft axis, (rad/sec)
ω_r	Frequency in r^{th} mode of vibration, (the imaginary part of λ_r), (rad/sec)
$\omega_\omega, \omega_\beta$	The natural frequencies of the uncoupled, undamped vibrations of the engine plus propeller about the gimbal mounting, in pitch and yaw respectively, (rad/sec)
ω_z, ω_y	The natural frequencies of the uncoupled, undamped vibrations of the engine plus propeller mass at the end of the cantilever nacelle with the gimbals locked, in vertical and horizontal translation respectively, (rad/sec)
$[]$	Brackets denoting a row matrix
{ }	Brackets denoting a column matrix

REFERENCES

No.	Author(s)	Title, etc.
1	W. H. Reed III and S. R. Bland	An analytical treatment of aircraft propeller precession instability. NASA Tech. Note No. D-659, January 1961.
2	H. S. Ribner	Propellers in yaw. NACA Report No. 820, 1945.
3	S. R. Bland and R. M. Bennett	Wind-tunnel measurement of propeller whirl-flutter speeds and static-stability derivatives and comparison with theory. NASA Tech. Note No. D-1807, August 1963.
4	F. T. Abbot, Jr. H. N. Kelly and K. D. Hampton	Investigation of propeller power-plant autoprecession boundaries for a dynamic-aeroelastic model of a four-engine turbo-prop transport airplane. NASA Tech. Note No. D-1806, August 1963.

APPENDIX A

Analysis of the Whirl Motion of an Engine Installation in Two Degrees of Freedom.

A.1. Engine mounted on fixed gimbals.

Equations of motion.

In this system the degrees of freedom allowed are the pitching and yawing rotations of the engine about a gimbal mounting fixed in space, (Fig. 24a).

In the absence of propeller aerodynamic forces, and with zero structural damping in the mounting, the Langrangian equations of motion are

$$\begin{aligned} I_\theta \ddot{\alpha}_1 + \Omega I_p \dot{\beta}_1 + K_\alpha \alpha_1 &= 0 \\ I_\psi \ddot{\beta}_1 - \Omega I_p \dot{\alpha}_1 + K_\beta \beta_1 &= 0. \end{aligned} \quad (\text{A.1})$$

Write

$$K_\alpha/I_\theta = \omega_\alpha^2 \text{ and } K_\beta/I_\psi = \omega_\beta^2$$

where ω_α and ω_β are the uncoupled natural frequencies of the system in pitch and yaw respectively.

Assuming solutions of the form $\alpha_1 = \dot{\alpha}_1 e^{j\lambda t}$ and $\beta_1 = \dot{\beta}_1 e^{j\lambda t}$ the equations of motion may be written in matrix form as

$$\begin{bmatrix} (\omega_\alpha^2 + \lambda^2) & \lambda \Omega I_p / I_\theta \\ -\lambda \Omega I_p / I_\psi & (\omega_\beta^2 + \lambda^2) \end{bmatrix} \begin{Bmatrix} \dot{\alpha}_1 \\ \dot{\beta}_1 \end{Bmatrix} = 0 \quad (\text{A.2})$$

Whirl mode frequencies.

For non-trivial solutions the determinant of the square matrix must vanish, which yields the following characteristic equation for λ :

$$\lambda^4 + \lambda^2 (\omega_\alpha^2 + \omega_\beta^2 + \Omega_1^2) + \omega_\alpha^2 \omega_\beta^2 = 0 \quad (\text{A.3})$$

where

$$\Omega_1 = \Omega \frac{I_p}{\sqrt{I_\theta I_\psi}}. \quad (\text{A.4})$$

Solutions of equation (A.3) are

$$\left. \begin{array}{l} \lambda_1^2 \\ \lambda_2^2 \end{array} \right\} = -\frac{1}{2} (\omega_\alpha^2 + \omega_\beta^2 + \Omega_1^2) \pm \frac{1}{2} \sqrt{(\omega_\alpha^2 + \omega_\beta^2 + \Omega_1^2)^2 - 4 \omega_\alpha^2 \omega_\beta^2}. \quad (\text{A.5})$$

The term inside the square root is always positive, hence λ^2 is real and negative. λ is therefore imaginary and may be written as $\lambda = i\omega$.

The system performs undamped simple harmonic motion in two modes, the frequencies of which are:

$$\left. \begin{array}{l} \omega_1^2 \\ \omega_2^2 \end{array} \right\} = \frac{1}{2} (\omega_\alpha^2 + \omega_\beta^2 + \Omega_1^2) \mp \frac{1}{2} \sqrt{(\omega_\alpha^2 + \omega_\beta^2 + \Omega_1^2)^2 - 4 \omega_\alpha^2 \omega_\beta^2}. \quad (\text{A.6})$$

The product of the frequencies reduces to the simple form

$$\omega_1 \omega_2 = \pm \omega_\alpha \omega_\beta$$

The expressions for ω_1 and ω_2 may be simplified as follows:

$$(\omega_1 + \omega_2)^2 \equiv \omega_1^2 + \omega_2^2 + 2\omega_1 \omega_2 = (\omega_\alpha + \omega_\beta)^2 + \Omega_1^2$$

Similarly

$$(\omega_1 - \omega_2)^2 \equiv \omega_1^2 + \omega_2^2 - 2\omega_1 \omega_2 = (\omega_\alpha - \omega_\beta)^2 + \Omega_1^2$$

Hence by addition and subtraction of these expressions we get

$$\begin{aligned} \omega_1 &= \pm \frac{1}{2} \left[\sqrt{(\omega_\alpha + \omega_\beta)^2 + \Omega_1^2} - \sqrt{(\omega_\alpha - \omega_\beta)^2 + \Omega_1^2} \right] \\ \omega_2 &= \pm \frac{1}{2} \left[\sqrt{(\omega_\alpha + \omega_\beta)^2 + \Omega_1^2} + \sqrt{(\omega_\alpha - \omega_\beta)^2 + \Omega_1^2} \right] \end{aligned} \quad (A.7)$$

Mode shapes.

The ratios of the amplitudes of the two degrees of freedom in each of the whirl modes may be found from equations (A.2). For mode r , putting $\lambda = i\omega_r$ the first of equations (A.2) yields

$$\left(\frac{\hat{\beta}_1}{\hat{\alpha}_1} \right)_r = i \left\{ \frac{\omega_\alpha^2 - \omega_r^2}{\Omega \omega_r I_p / I_\theta} \right\} \quad (A.8)$$

while from the second of equations (A.2)

$$\left(\frac{\hat{\beta}_1}{\hat{\alpha}_1} \right)_r = i \left\{ \frac{\Omega \omega_r I_p / I_\psi}{\omega_\beta^2 - \omega_r^2} \right\} \quad (A.9)$$

Assuming that $\omega_\beta > \omega_\alpha$, equation (A.7) indicates that in mode 1, $\omega_1 \leq \omega_\alpha$, and the motion is then a backward whirl in which the propeller hub describes an elliptical orbit in the y,z plane in a direction opposite to the propeller rotation. In mode 2, $\omega_2 \geq \omega_\beta$ and the motion is a forward whirl in the same sense as the propeller rotation.

The amplitude ratio may be expressed in a form independent of Ω by multiplying together equations (A.8) and (A.9) and taking the square root:

$$\left\{ \frac{\hat{\beta}_1}{\hat{\alpha}_1} \right\}_r = \pm i \sqrt{\frac{I_\theta (\omega_\alpha^2 - \omega_r^2)}{I_\psi (\omega_\beta^2 - \omega_r^2)}} \quad (A.10)$$

When expressed in this form the mode shapes, as determined from the amplitude ratios of the separate degrees of freedom, are seen not to be directly dependent on Ω and I_p .

A.2. Engine mounted on a cantilever nacelle.

Equations of motion.

In this system the engine is assumed to be rigidly attached to the end of a nacelle structure which is encastré at the root and free to deflect in the vertical and horizontal planes in the fundamental cantilever bending modes. The slopes at the end of the nacelle are assumed to be proportional to the relevant displacements, (Fig. 24b).

The Langrangian equations of motion may be written as:

$$\left. \begin{aligned} (m_E + I_\theta r_\theta^2) \ddot{z}_1 - \Omega I_P r_\theta r_\psi \dot{y}_1 + K_z z_1 &= 0 \\ (m_E + I_\psi r_\psi^2) \ddot{y}_1 + \Omega I_P r_\psi r_\theta \dot{z}_1 + K_y y_1 &= 0 \end{aligned} \right\} \quad (\text{A.11})$$

Now let

$$K_z/(m_E + I_\theta r_\theta^2) = \omega_z^2 \quad \text{and} \quad K_y/(m_E + I_\psi r_\psi^2) = \omega_y^2$$

where ω_z and ω_y are the uncoupled natural frequencies of the system in the vertical and horizontal planes.

Then assuming solutions of the form

$$z_1 = \hat{z}_1 e^{\lambda t} \quad \text{and} \quad y_1 = \hat{y}_1 e^{\lambda t},$$

the equations of motion may be written in matrix form as:

$$\begin{bmatrix} (\omega_z^2 + \lambda^2) & -\Omega \lambda \left(\frac{I_P r_\theta r_\psi}{m_E + I_\theta r_\theta^2} \right) \\ \Omega \lambda \left(\frac{I_P r_\theta r_\psi}{m_E + I_\psi r_\psi^2} \right) & (\omega_y^2 + \lambda^2) \end{bmatrix} \begin{Bmatrix} \hat{z}_1 \\ \hat{y}_1 \end{Bmatrix} = 0. \quad (\text{A.12})$$

Whirl mode frequencies.

The characteristic equation for λ is

$$\lambda^4 + \lambda^2 (\omega_z^2 + \omega_y^2 + \Omega_2^2) + \omega_z^2 \omega_y^2 = 0 \quad (\text{A.13})$$

where

$$\Omega_2 = \Omega \left\{ \frac{I_P r_\theta r_\psi}{\sqrt{(m_E + I_\theta r_\theta^2)(m_E + I_\psi r_\psi^2)}} \right\}. \quad (\text{A.14})$$

Equation (A.13) is identical in form to equation (A.3), with ω_z and ω_y replacing ω_x and ω_β and with Ω_2 replacing Ω_1 . With these substitutions the binary whirl mode frequencies are given by equations (A.7).

Mode shapes.

From equations (A.12) the amplitude ratio of the degrees of freedom in each whirl mode may be written as

$$\begin{aligned} \left\{ \frac{\hat{y}_1}{\hat{z}_1} \right\}_r &= -i \left\{ \frac{\omega_z^2 - \omega_r^2}{\Omega \omega_r} \cdot \frac{m_E + I_\theta r_\theta^2}{I_P r_\theta r_\psi} \right\} \\ &= -i \left\{ \frac{\Omega \omega_r}{\omega_y^2 - \omega_r^2} \cdot \frac{I_P r_\theta r_\psi}{m_E + I_\psi r_\psi^2} \right\} \end{aligned} \quad (\text{A.15})$$

Assuming that $\omega_y > \omega_z$ then equation (A.7) indicates that $\omega_1 \leq \omega_z$ and equations (A.15) show that the mode 1 is a backward whirl motion, with the tip of the nacelle tracing an elliptical path in the y,z plane against the direction of the propeller rotation. Conversely $\omega_2 \geq \omega_y$, and mode 2 is a forward whirl motion.

The amplitude ratio may be expressed in a form not directly dependent on Ω or I_p :

$$\left\{ \begin{array}{l} \hat{y}_1 \\ \hat{z}_1 \end{array} \right\}_r = \pm i \sqrt{\left(\frac{\omega_z^2 - \omega_r^2}{\omega_y^2 - \omega_r^2} \right) \left(\frac{m_E + I_\theta r_\theta^2}{m_E + I_\psi r_\psi^2} \right)} . \quad (\text{A.16})$$

A.3. General expression for binary whirl mode frequencies.

In the absence of aerodynamic forces on structural damping the equations of motion for the binary systems in either the engine or the nacelle freedoms are identical in form when expressed in terms of suitable parameters. The two systems may therefore be regarded as equivalent.

The whirl mode frequencies may be written in the following dimensionless forms:

$$\left\{ \begin{array}{l} \frac{\omega_1}{\underline{\Omega}} \\ \frac{\omega_2}{\underline{\Omega}} \end{array} \right\} = \frac{1}{2} \left\{ \sqrt{1 + \left(\frac{\omega_{\min}}{\underline{\Omega}} \right)^2 (1+k)^2} \mp \sqrt{1 + \left(\frac{\omega_{\min}}{\underline{\Omega}} \right)^2 (k-1)^2} \right\} \quad (\text{A.17})$$

or

$$\left\{ \begin{array}{l} \frac{\omega_1}{\omega_{\min}} \\ \frac{\omega_2}{\omega_{\min}} \end{array} \right\} = \frac{1}{2} \left\{ \sqrt{(k+1)^2 + \left(\frac{\underline{\Omega}}{\omega_{\min}} \right)^2} \mp \sqrt{(k-1)^2 + \left(\frac{\underline{\Omega}}{\omega_{\min}} \right)^2} \right\} \quad (\text{A.18})$$

where ω_1 and ω_2 are the frequencies of the backward and forward whirl modes respectively

ω_{\min} is the lesser of the two uncoupled natural frequencies of the system with $\Omega = 0$

ω_{\max} is the greater of the two uncoupled frequencies

$k = \omega_{\max}/\omega_{\min}$

$\underline{\Omega} = \Omega_1$ for a binary in the engine freedoms

and $\underline{\Omega} = \Omega_2$ for a binary in the nacelle freedoms

Equations (A.17) and (A.18) are plotted in Fig. 25.

TABLE 1

Basic Data for Engine-nacelle Installations, used in Forming the Flutter Matrices.

Quantity	Units	Inboard installation	Outboard installation
m_E	slugs	100.6	100.6
I_θ	slugs ft ²	780	780
I_ψ	slugs ft ²	780	780
I_P	slugs ft ²	280	280
x_G	ft	14.33	12.71
x_E	ft	14.46	12.84
x_P	ft	17.11	15.49
x_L	ft	3.08	2.71
l_E	ft	0.125	0.125
l_P	ft	2.78	2.78
r_θ	rad/ft	0.178	0.200
r_ψ	rad/ft	0.178	0.200
c_m	ft	12.96	12.96
Ω	rad/sec	-102.2	-102.2
Ω_1	rad/sec	-36.65	-36.65
Ω_2	rad/sec	-7.25	-8.70
K_z	lb/ft	21.1×10^4	15.5×10^4
K_α	lb ft/rad	60.0×10^4	61.5×10^4
K_y	lb/ft	14.9×10^4	10.7×10^4
K_β	lb ft/rad	63.3×10^4	60.2×10^4

TABLE 2

Propeller Data and Aerodynamic Derivatives.

Propeller diameter = 14.5 ft
 Engine rotational speed = - 15250 rev/min
 Propeller rotational speed $N = - 16.25$ rev/sec
 $\Omega = - 102.2$ rad/sec

N.B. Positive rotation is in accordance with the right hand rule, i.e. clockwise when viewed from aft.

Derivative	$J = 1$	$J = 2$	$J = 3$
$C_{y\psi}$	0.310	0.364	0.410
$C_{z\psi}$	-0.067	-0.071	-0.075
C_{mq}	-0.143	-0.072	-0.040
$C_{m\psi}$	-0.126	-0.127	-0.111
C_{yq}	0.243	0.246	0.220
$C_{z\theta}$	-0.310	-0.364	-0.410
$C_{y\theta}$	-0.067	-0.071	-0.075
C_{nr}	-0.143	-0.072	-0.040
$C_{n\theta}$	0.126	0.127	0.111
C_{zr}	0.243	0.246	0.220

$$J = \frac{V}{2NR} = 0.00424 V \quad (\text{with } V \text{ in ft/sec})$$

The above derivatives are for a non-thrusting propeller.

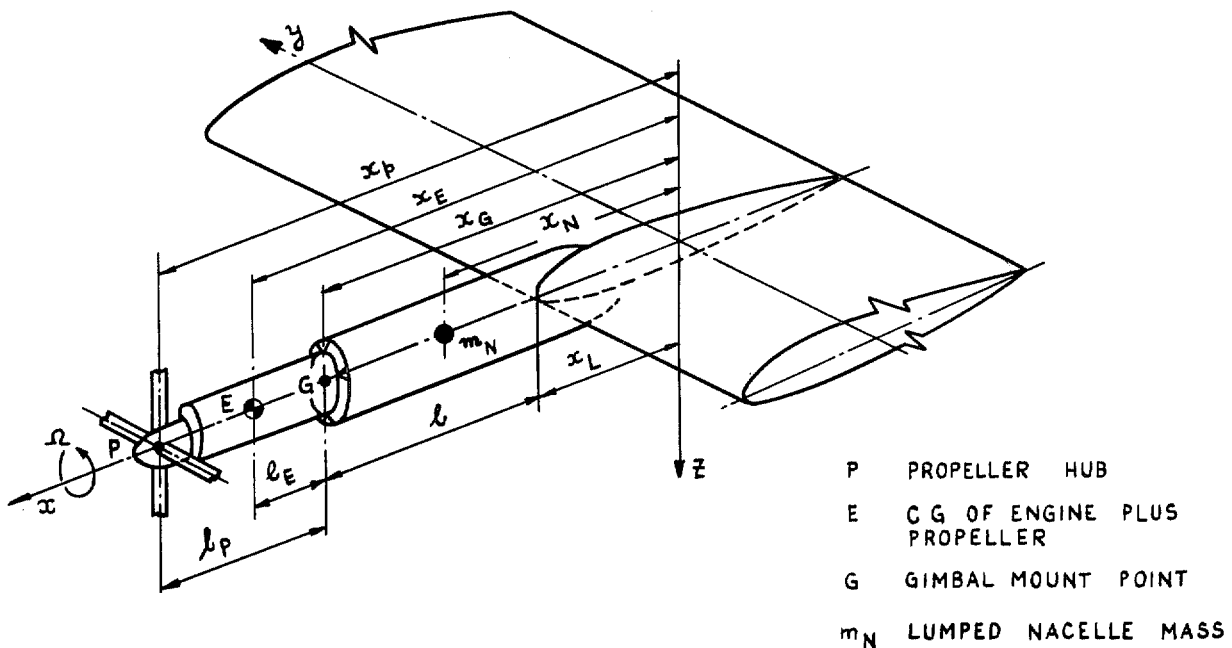
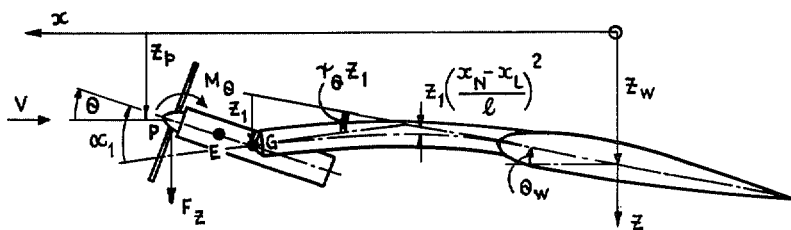
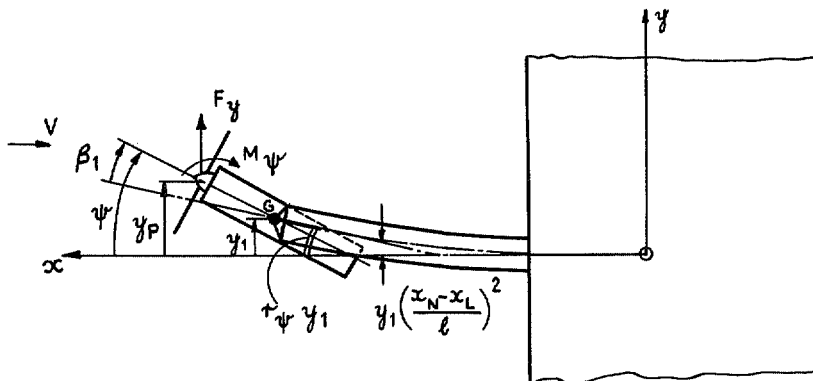


FIG. 1. Geometry of engine/nacelle installation.



DISPLACEMENTS AND AERODYNAMIC FORCES IN PITCH PLANE



DISPLACEMENTS AND AERODYNAMIC FORCES IN YAW PLANE

FIG. 2. Displacements and propeller aerodynamic forces for nacelle-engine installation.

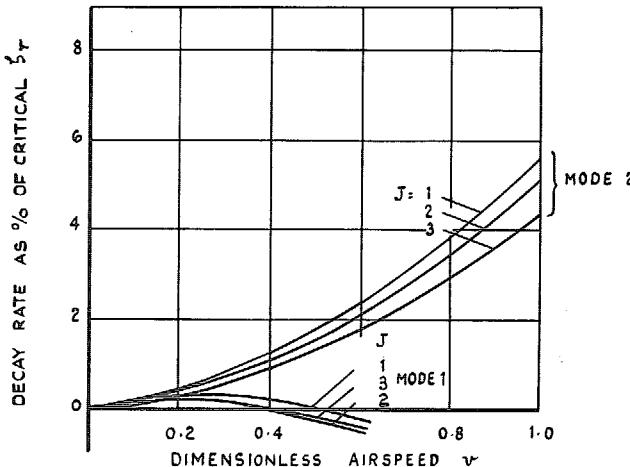
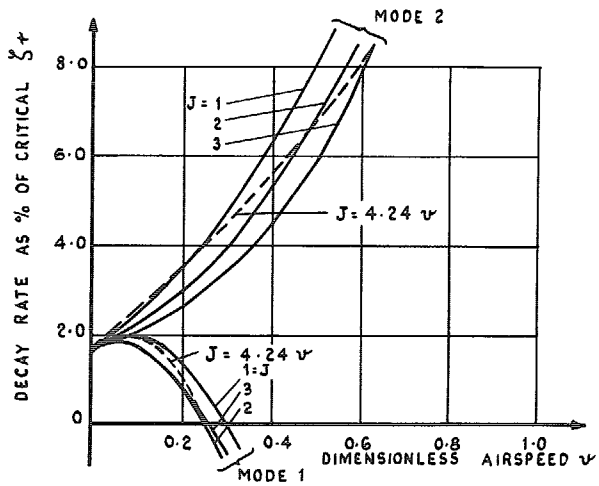
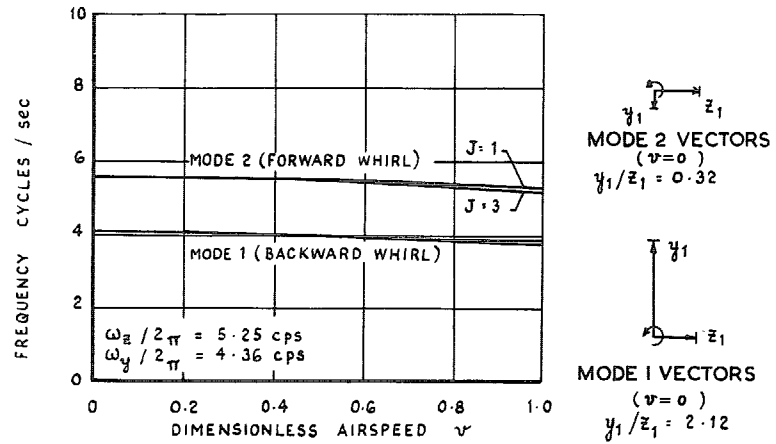
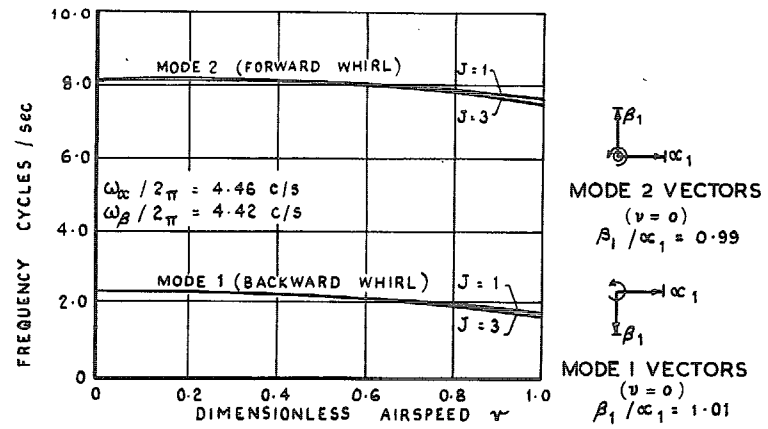


FIG. 3. Whirl of outboard engine in 2 degrees of freedom. Variation of whirl-mode frequencies and decay rates with airspeed.

FIG. 4. Whirl of outboard nacelle in 2 degrees of freedom. Variation of whirl - mode frequencies and decay rates with airspeed.

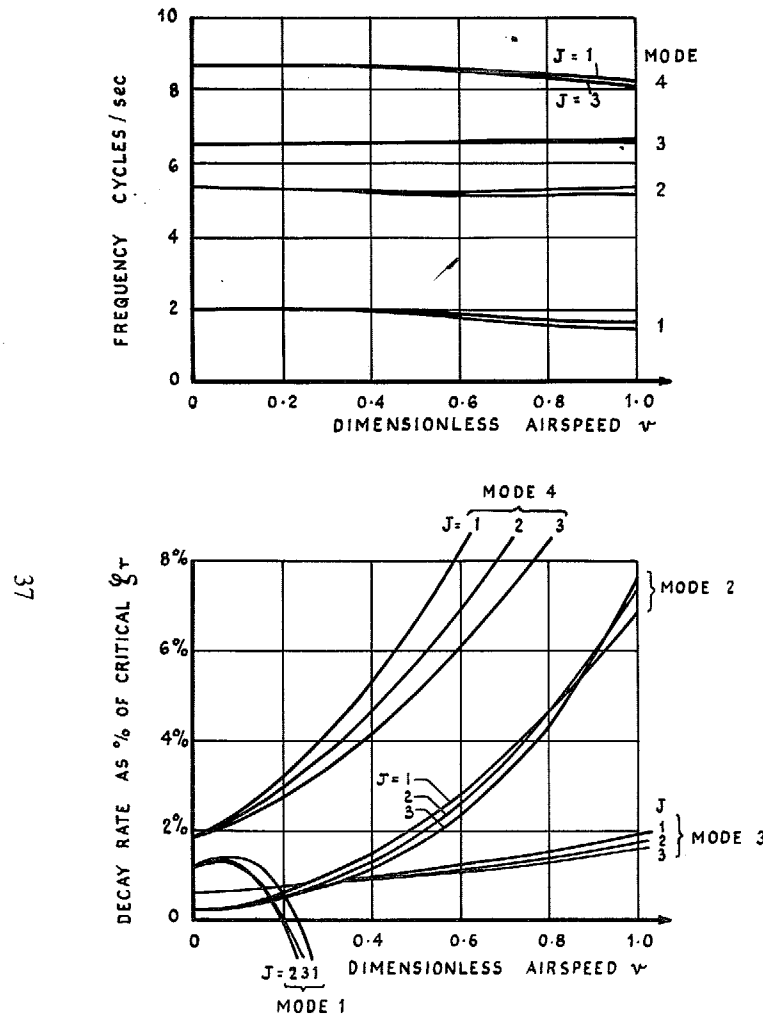
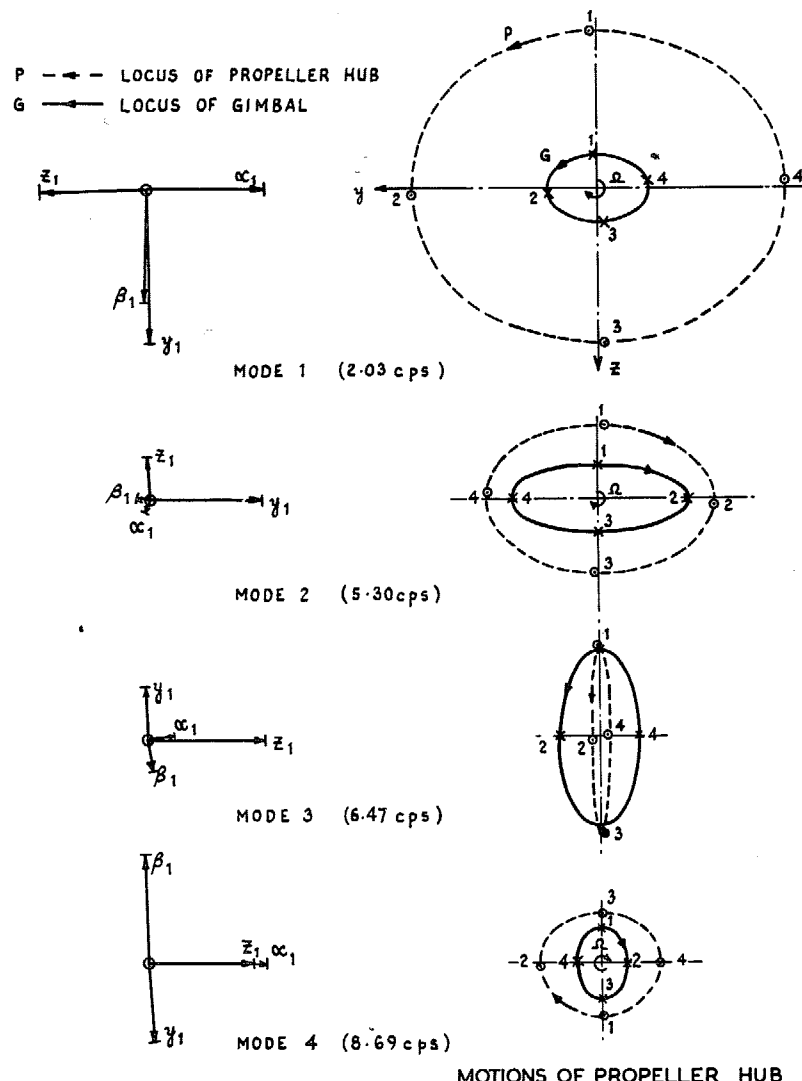


FIG. 5. Whirl of outboard nacelle-engine installation in 4 degrees of freedom. Variation of whirl-mode frequencies and damping rates with airspeed.



VECTOR DIAGRAMS MOTIONS OF PROPELLER HUB AND GIMBAL POINT

FIG. 6. Whirl of outboard nacelle-engine installation in 4 degrees of freedom ($v = 0, J = 2$).

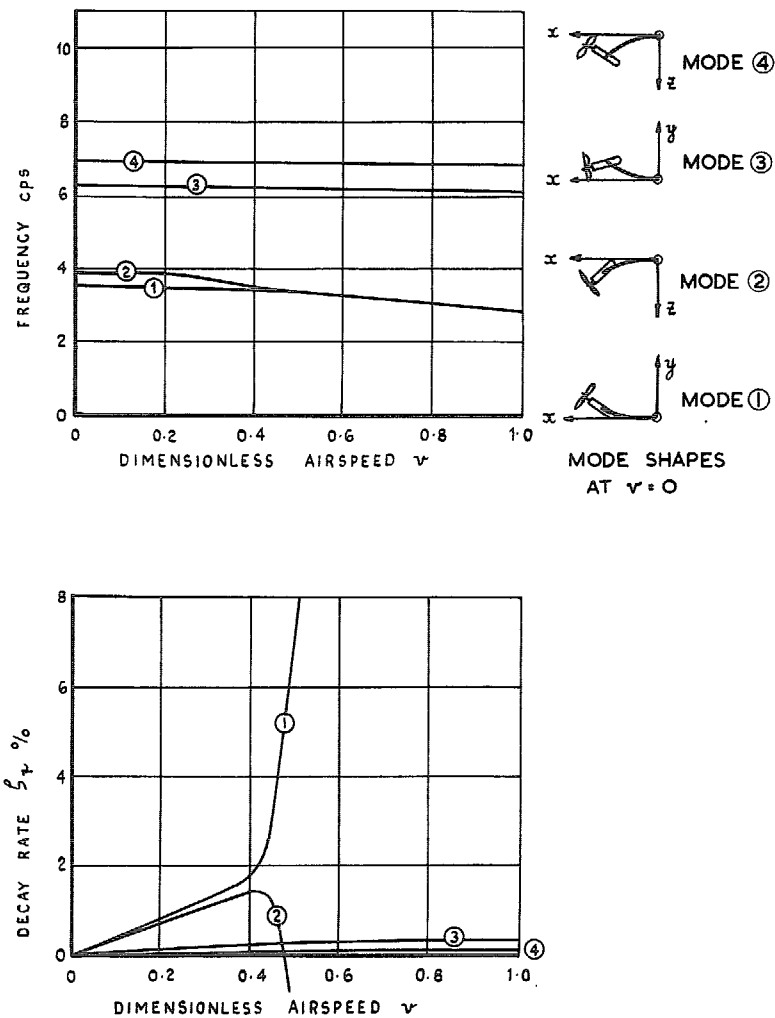


FIG. 7. Whirl of outboard installation in 4 degrees of freedom. (Gyroscopic effects omitted).

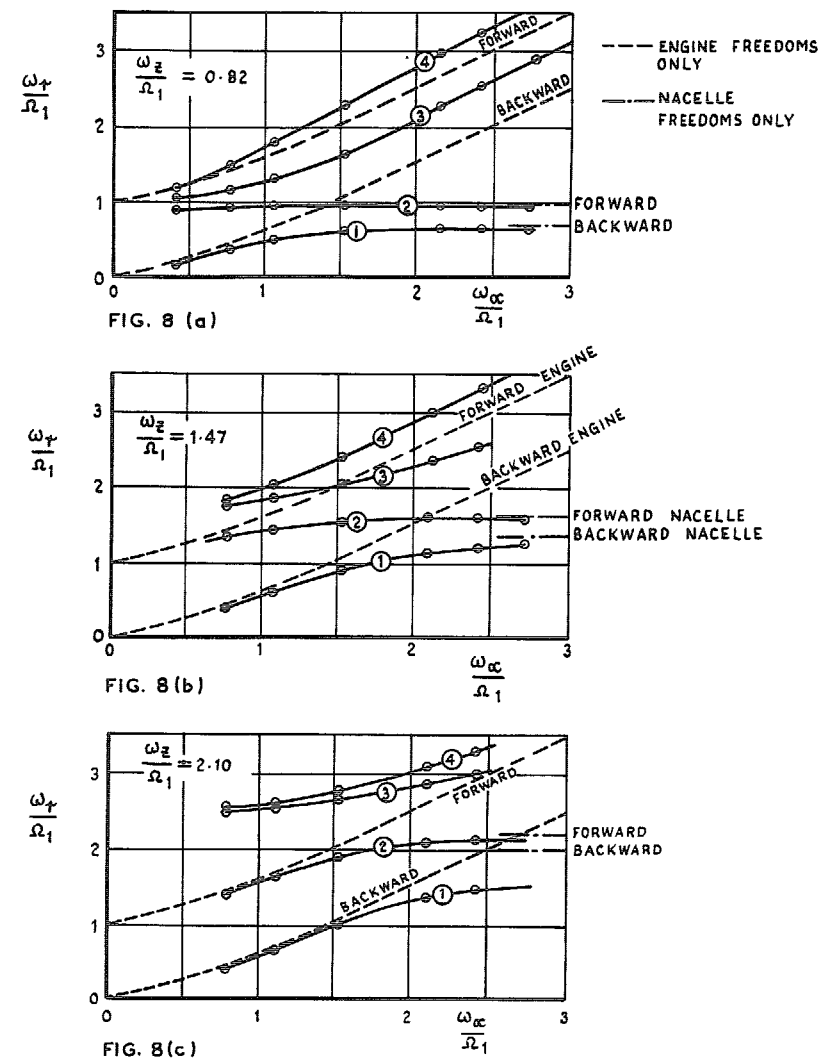


FIG. 8. Whirl of nacelle-engine installation in 4 degrees of freedom. Whirl mode frequencies against engine-mount frequency.

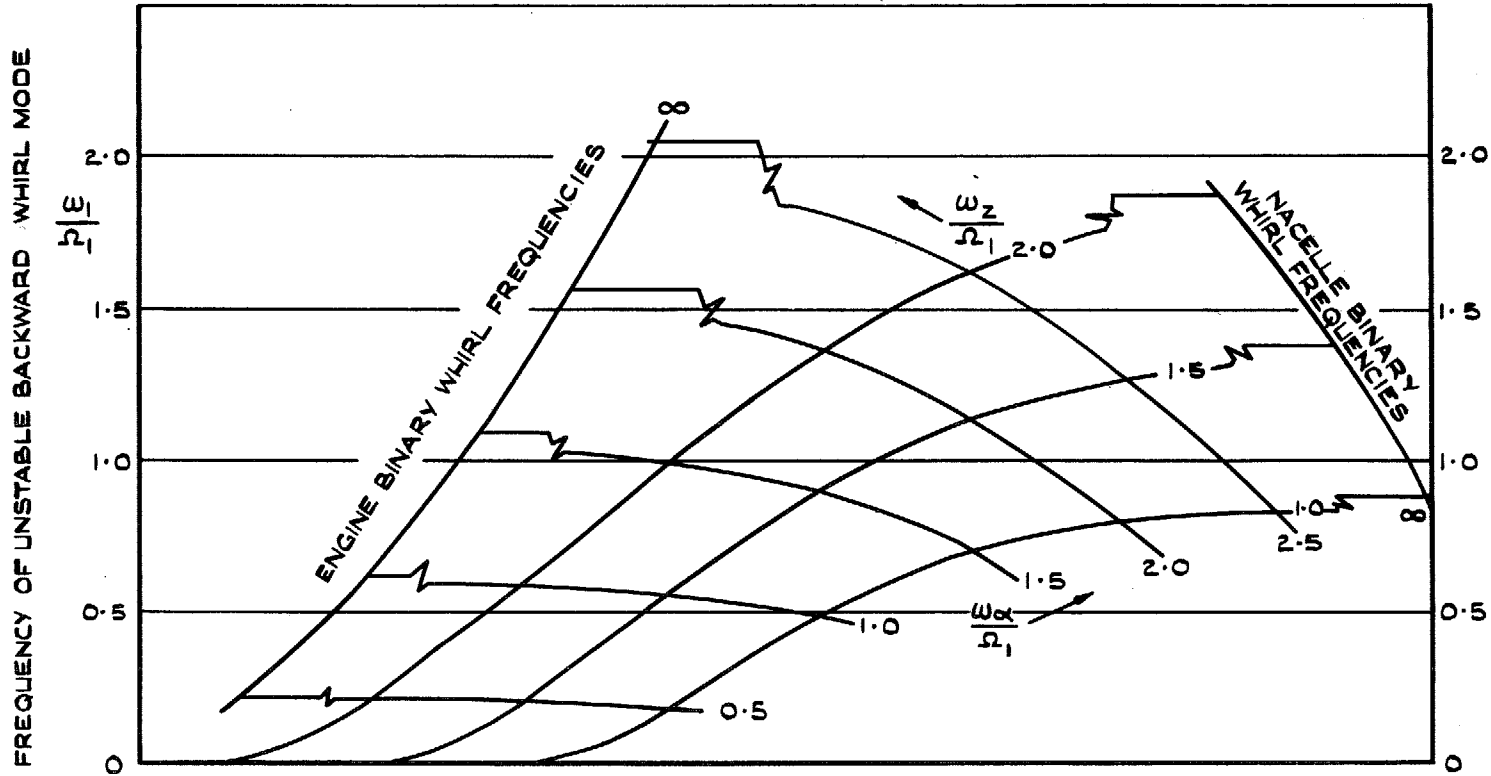


FIG. 9. Whirl of nacelle-engine installation in 4 degrees of freedom. Zero airspeed frequency of unstable backward whirl mode 1 as a function of the uncoupled natural frequencies of the nacelle and engine.

	CASE (a)	CASE (b)	CASE (c)	CASE (d)
$\frac{\omega_e}{\Omega_1}$	2.10	2.10	0.82	0.82
$\frac{\omega_{ac}}{\Omega_1}$	0.76	1.52	0.76	1.52
MODE 1				
$\frac{\omega_e}{\Omega_1}$	0.401	1.005	0.348	0.599
MODE 2				
$\frac{\omega_e}{\Omega_1}$	1.388	1.888	0.910	0.948
MODE 3				
$\frac{\omega_e}{\Omega_1}$	2.479	2.635	1.108	1.609
MODE 4				
$\frac{\omega_e}{\Omega_1}$	2.492	2.750	1.487	2.277

FIG. 10. Whirl of nacelle-engine installation in 4 degrees of freedom. Vector diagrams for whirl modes at zero airspeed for various nacelle and engine stiffnesses.

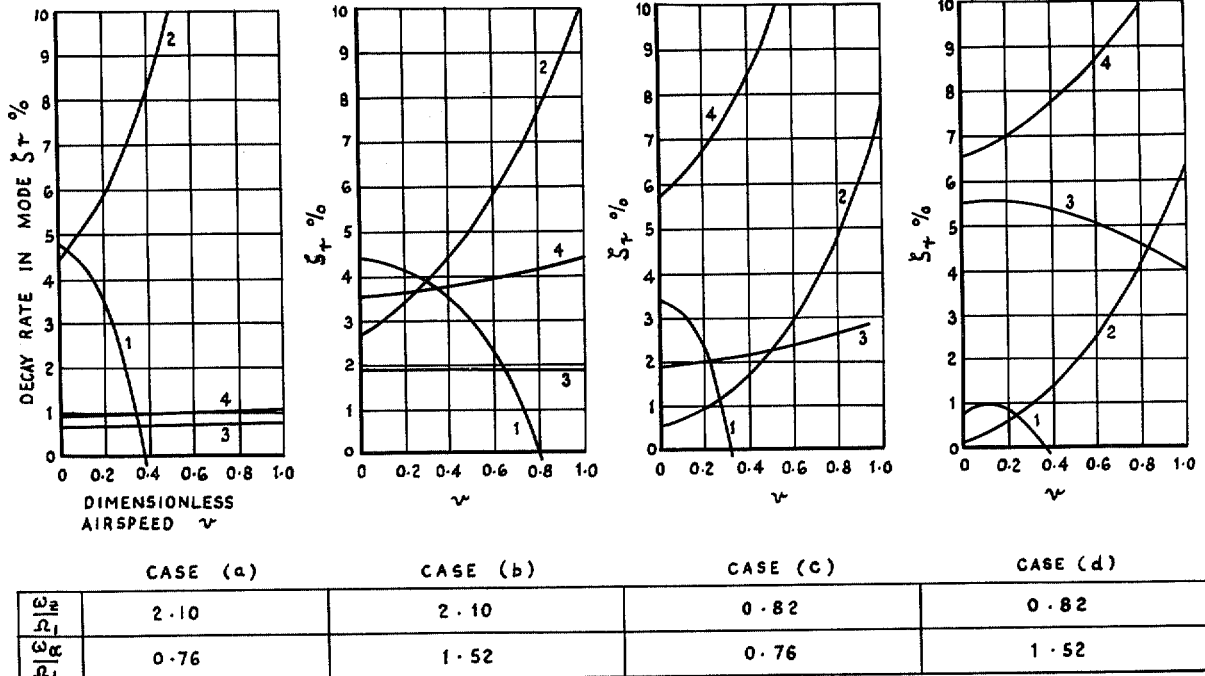


FIG. 11. Whirl of nacelle-engine installation in 4 degrees of freedom. Decay rate in whirl modes as a function of airspeed.

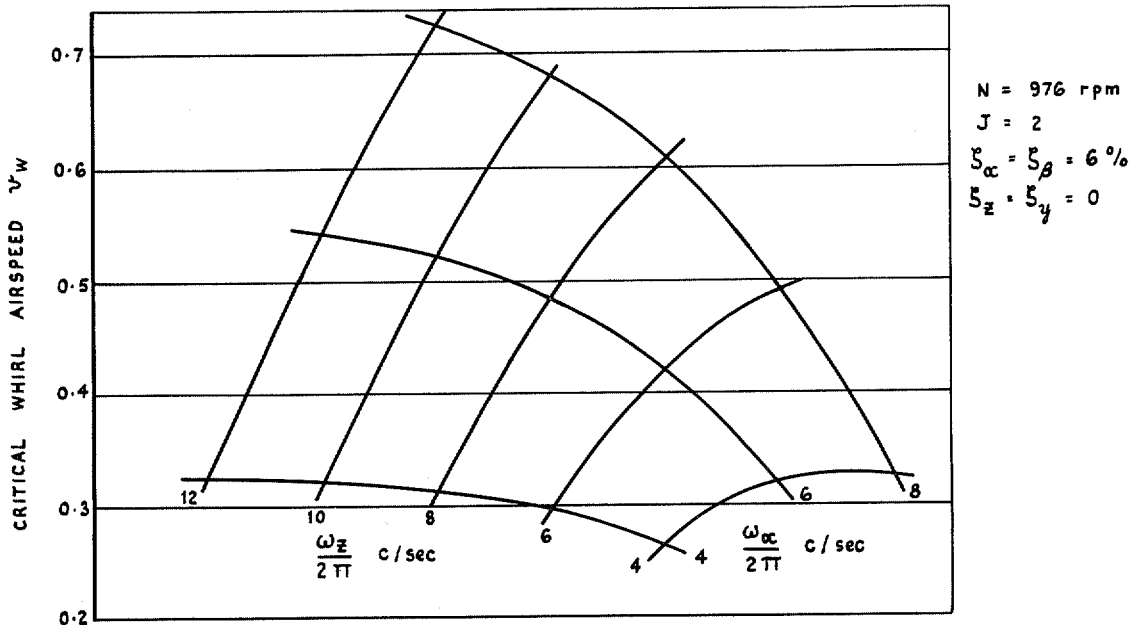


FIG. 12. Whirl of nacelle-engine installation in 4 degrees of freedom. Critical whirl airspeed in terms of nacelle and engine mount frequencies.

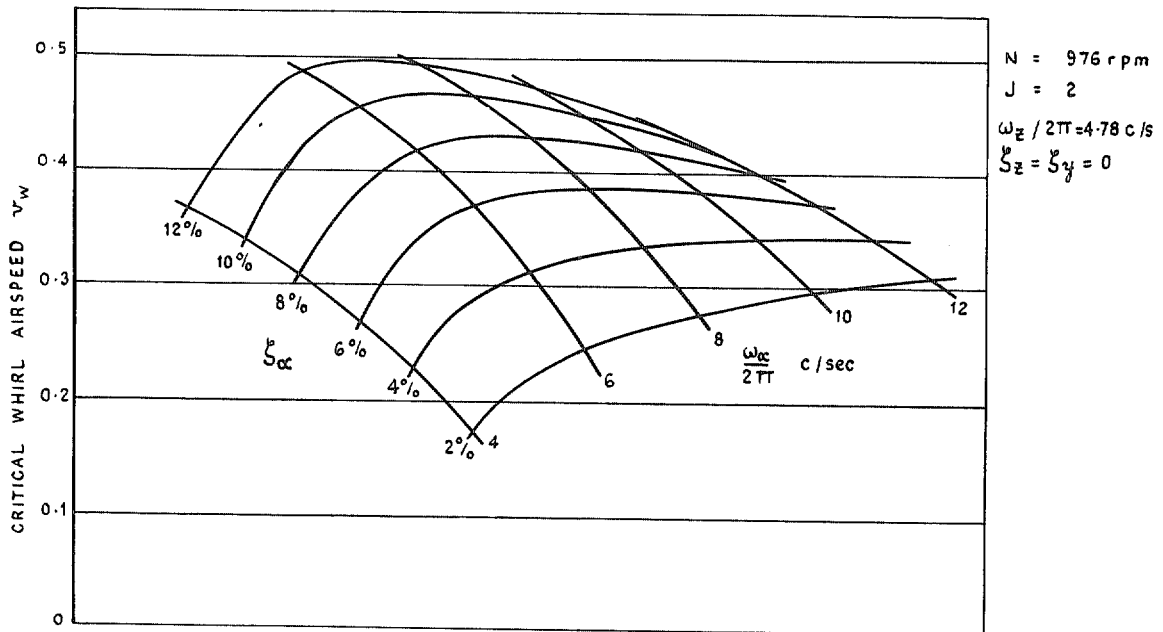


FIG. 13. Whirl of nacelle-engine installation in 4 degrees of freedom. Critical whirl airspeed in terms of engine-mount frequency and structural damping coefficient.

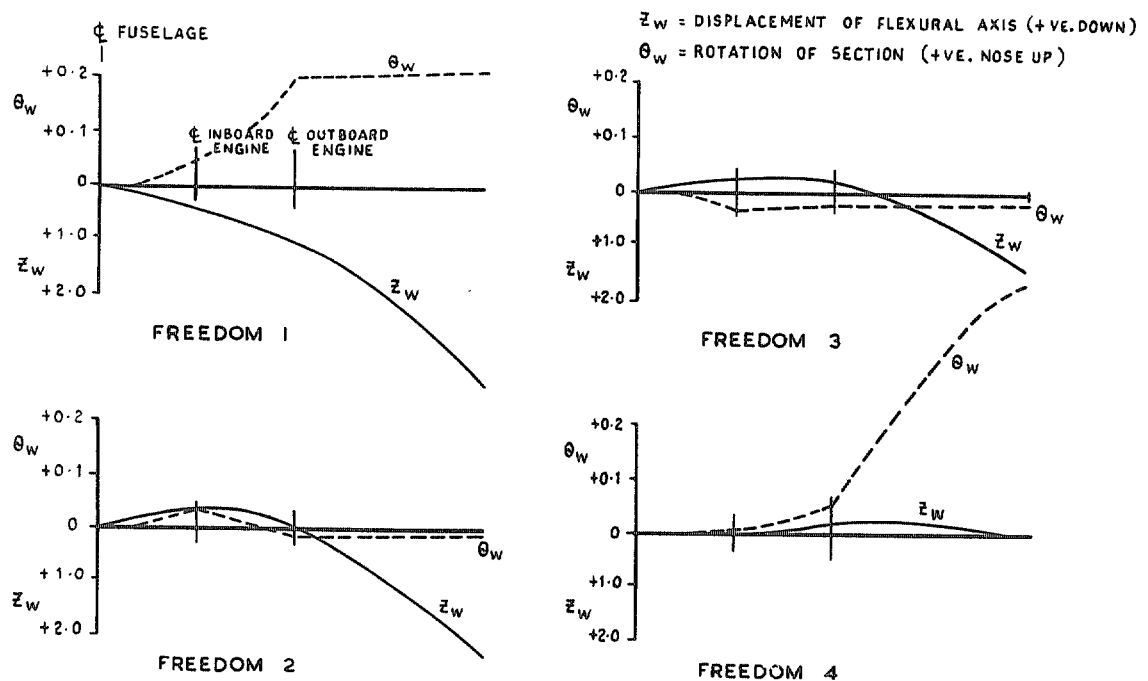
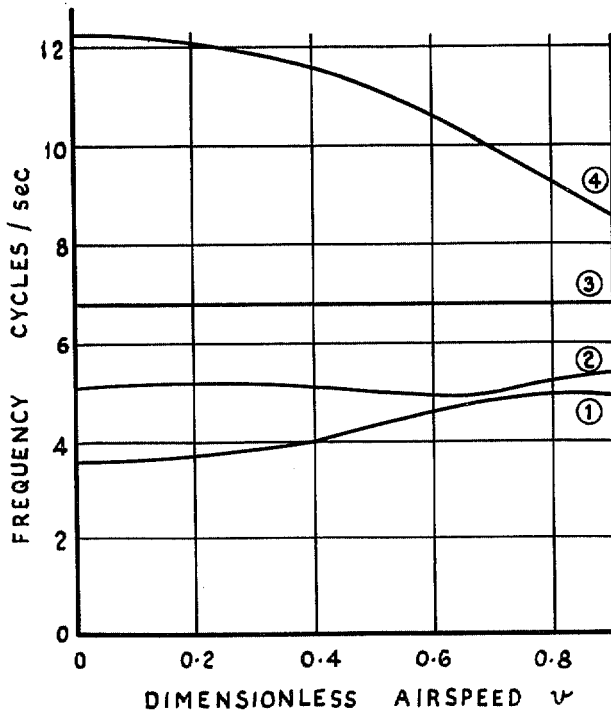
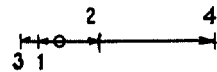


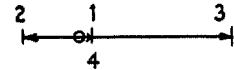
FIG. 14. Degrees of freedom allocated to wing.



MODE VECTORS



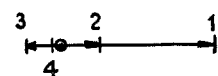
MODE ④ ($v = 0$)



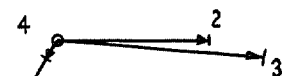
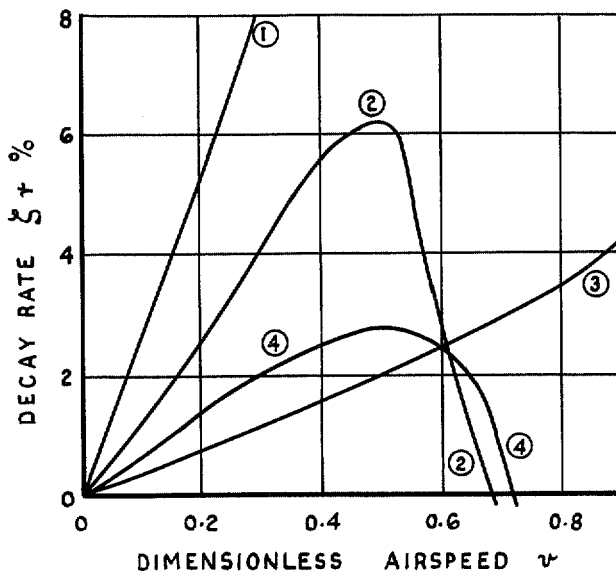
MODE ③ ($v = 0$)



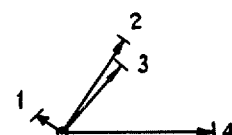
MODE ② ($v = 0$)



MODE ① ($v = 0$)



MODE ② ($v = 0.685$)



MODE ④ ($v = 0.720$)

FIG. 15. Flutter of wing with rigid engine installations. Mode frequencies and decay rates against airspeed.

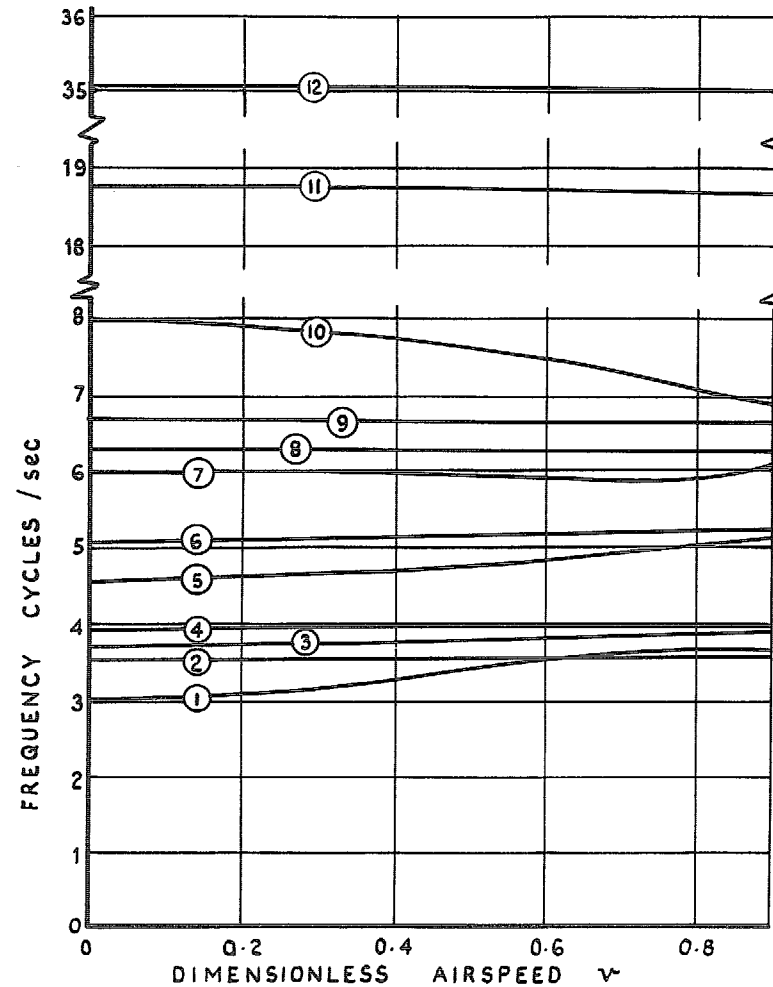
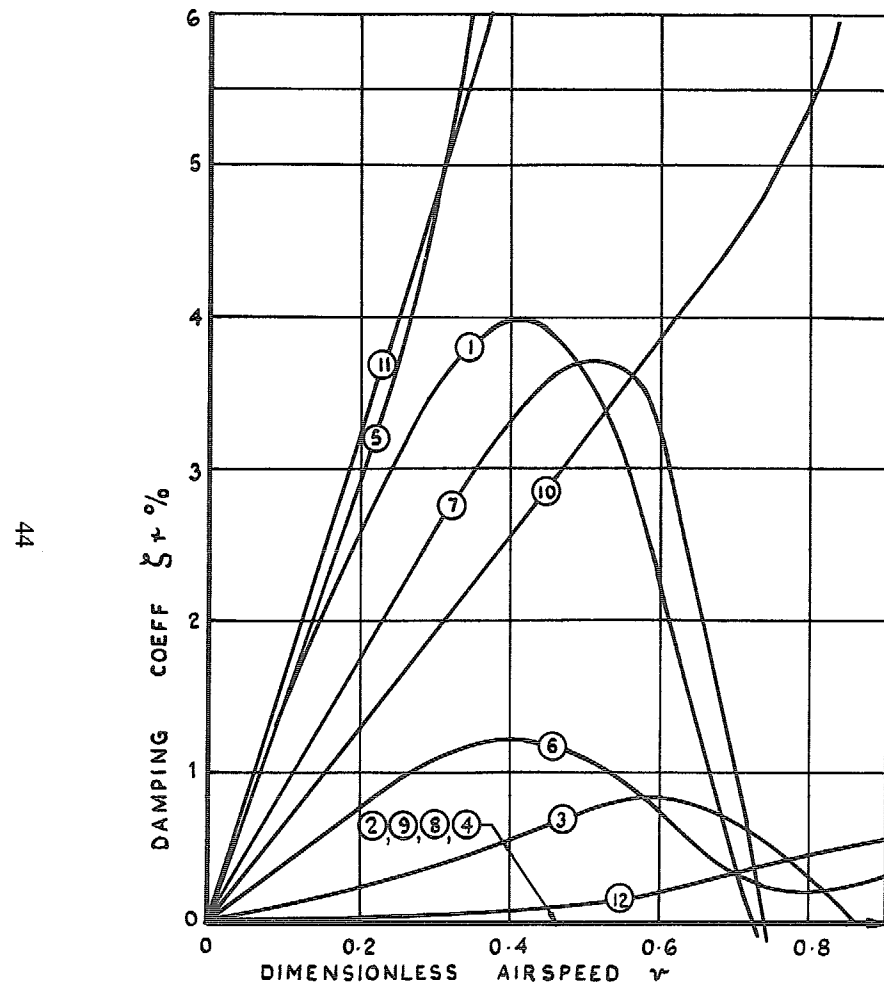


FIG. 16. Flutter of wing with flexible engine installations. Propeller aerodynamics and gyroscopic effects ignored.

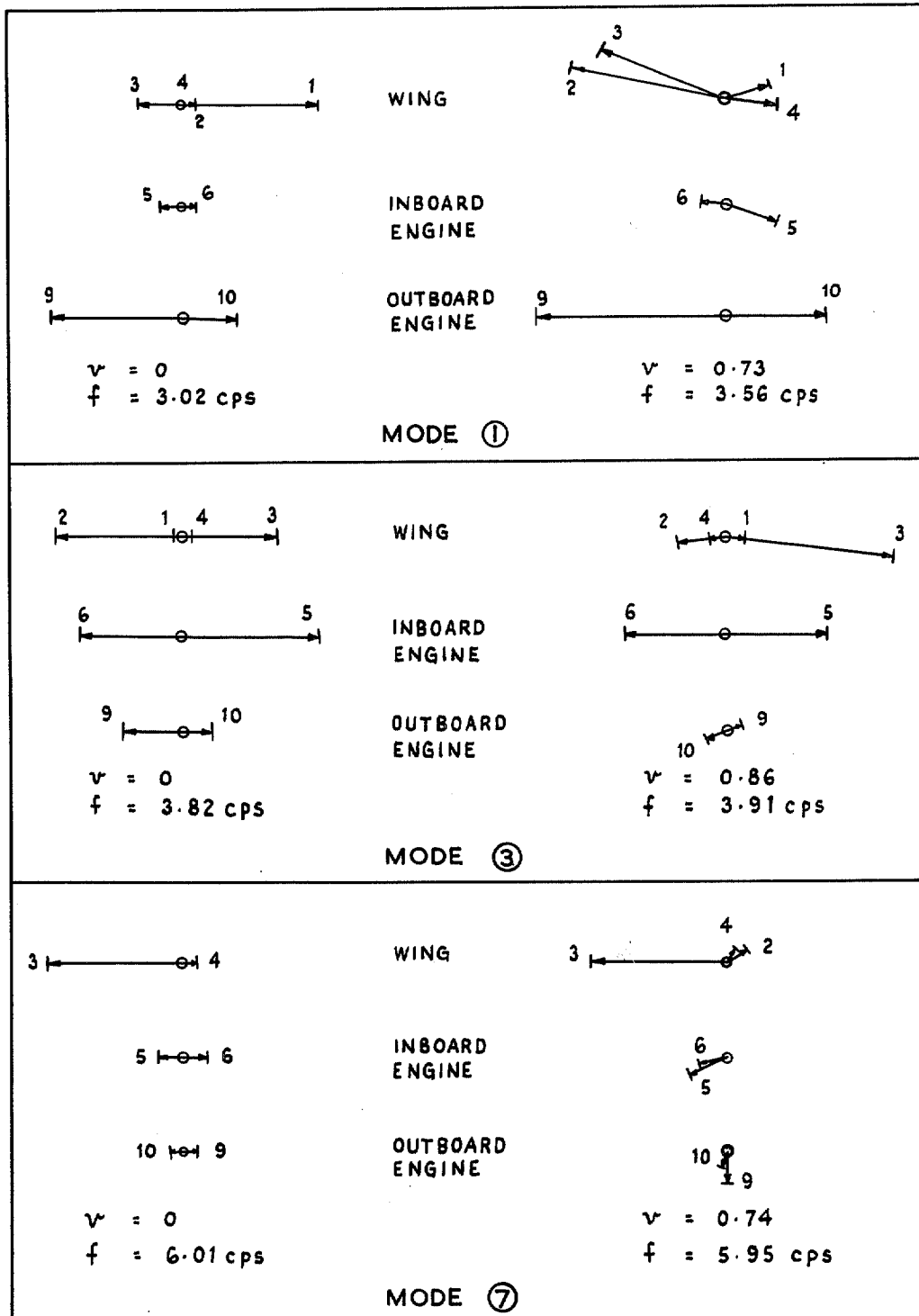


FIG. 17. Flutter-mode vectors for wing plus flexible engine installations. (Propeller effects ignored).

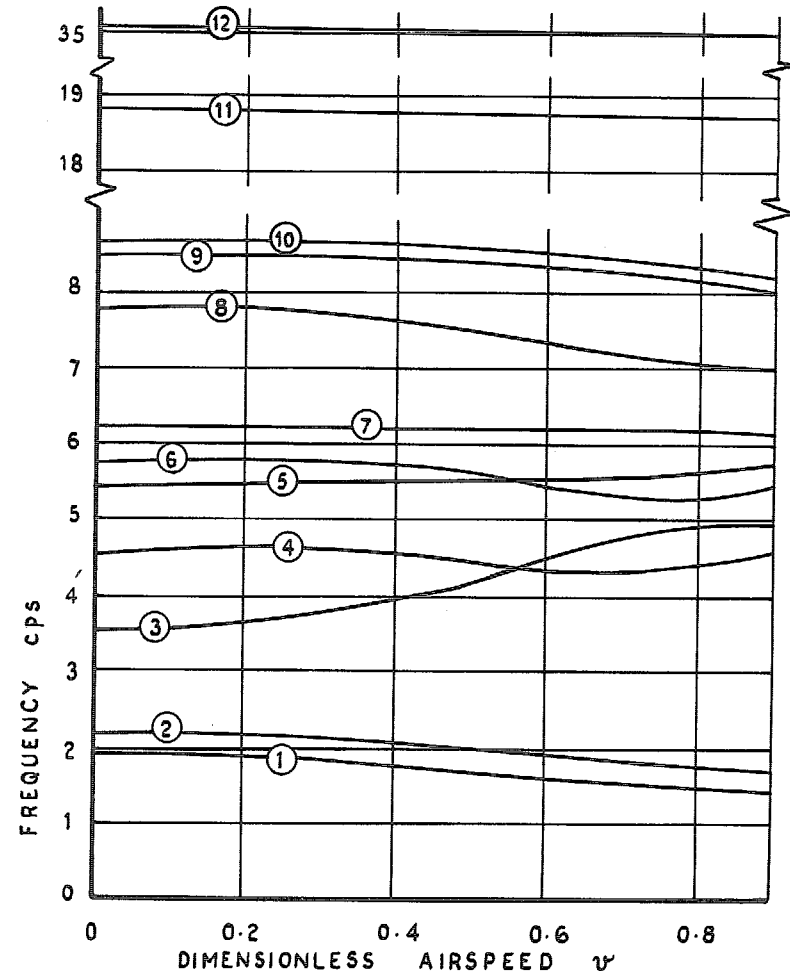
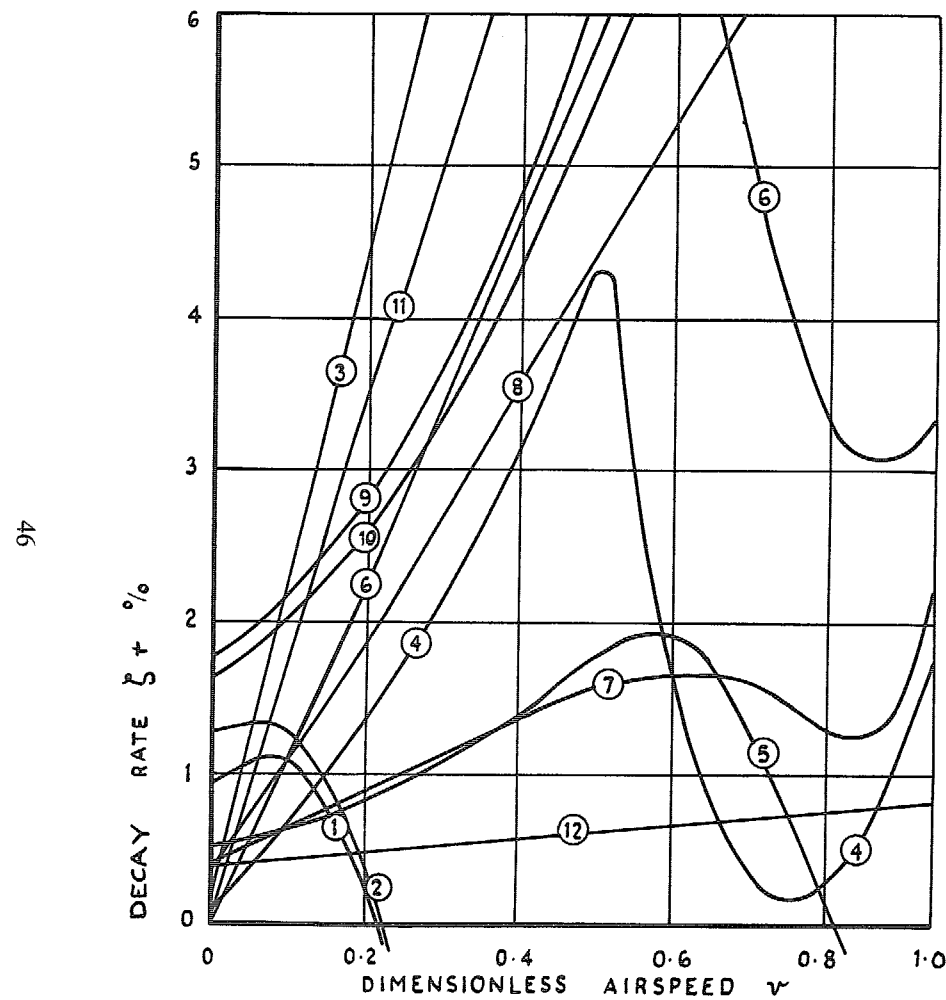


FIG. 18. Flutter of wing with flexible engine installations. Propeller aerodynamic and gyroscopic effects included.

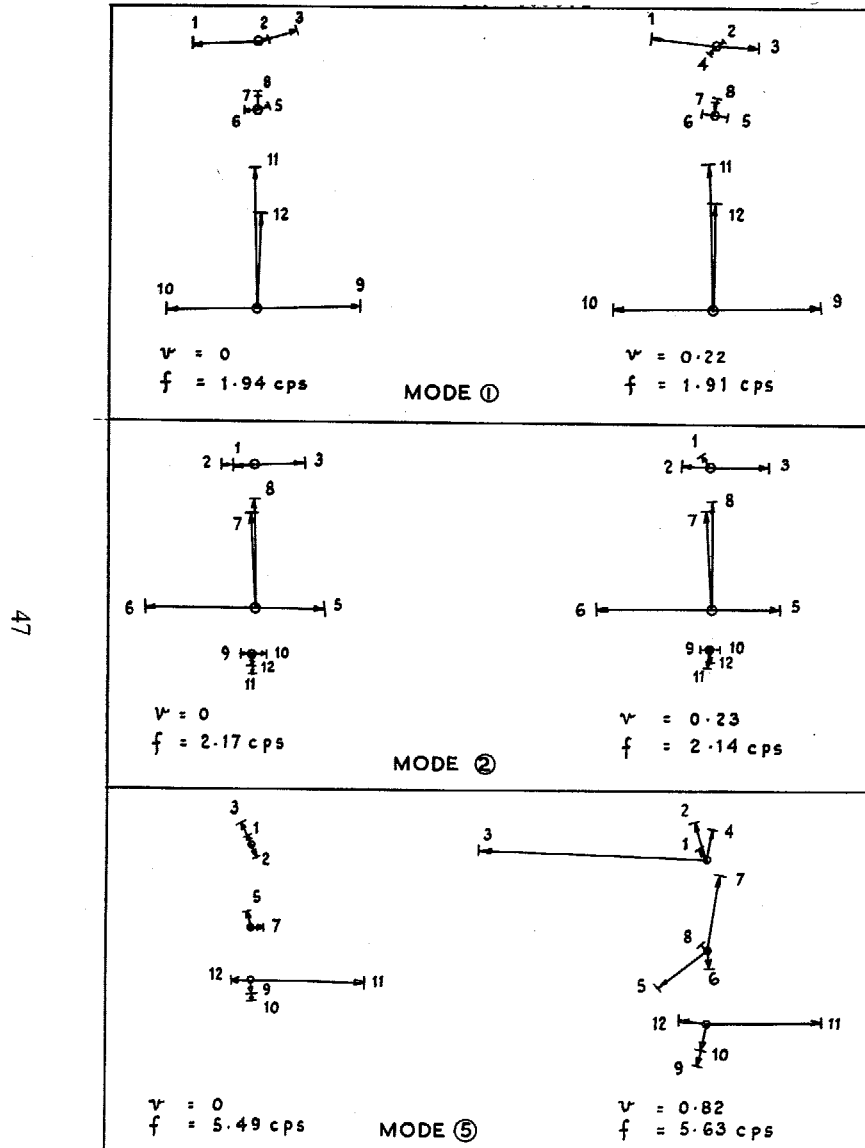


FIG. 19. Unstable-mode vectors for wing with flexible installations (propeller effects included).

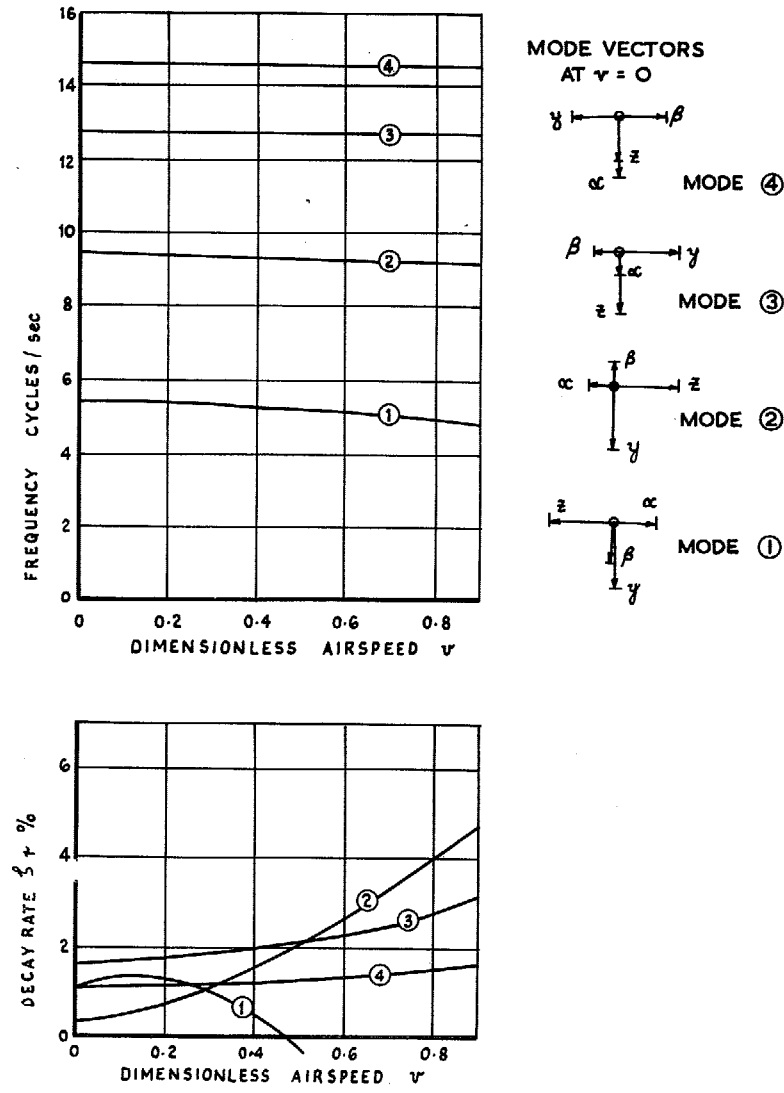


FIG. 20. Whirl of stiffened outboard nacelle-engine installation in 4 degrees of freedom.

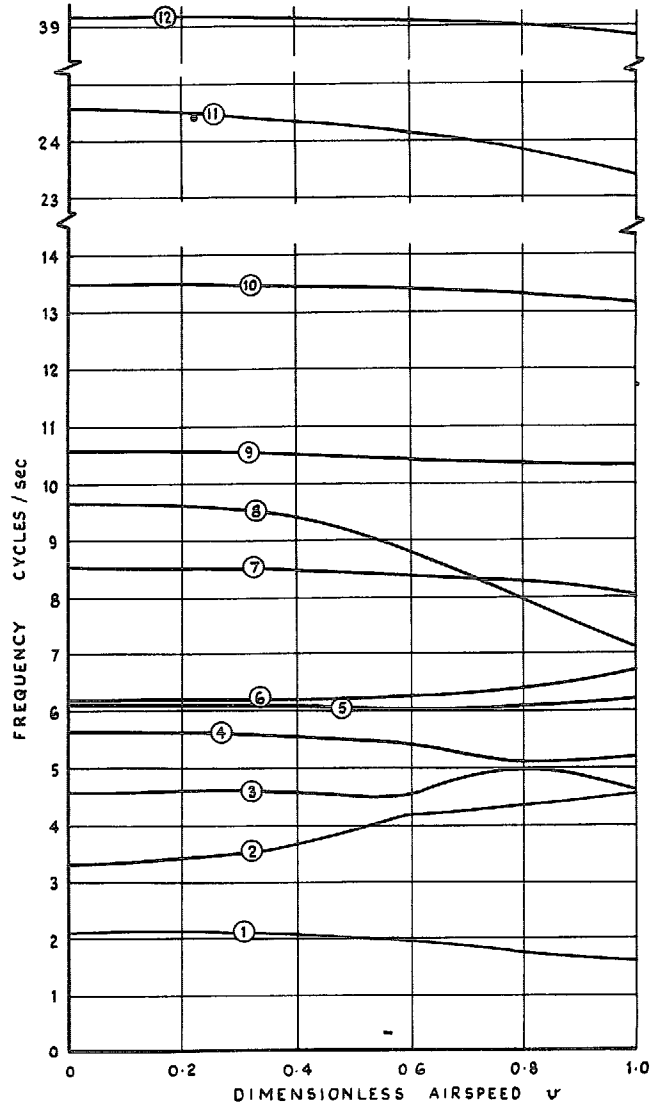


FIG. 21. Flutter of wing with stiffened outboard installation. Mode frequencies against airspeed.

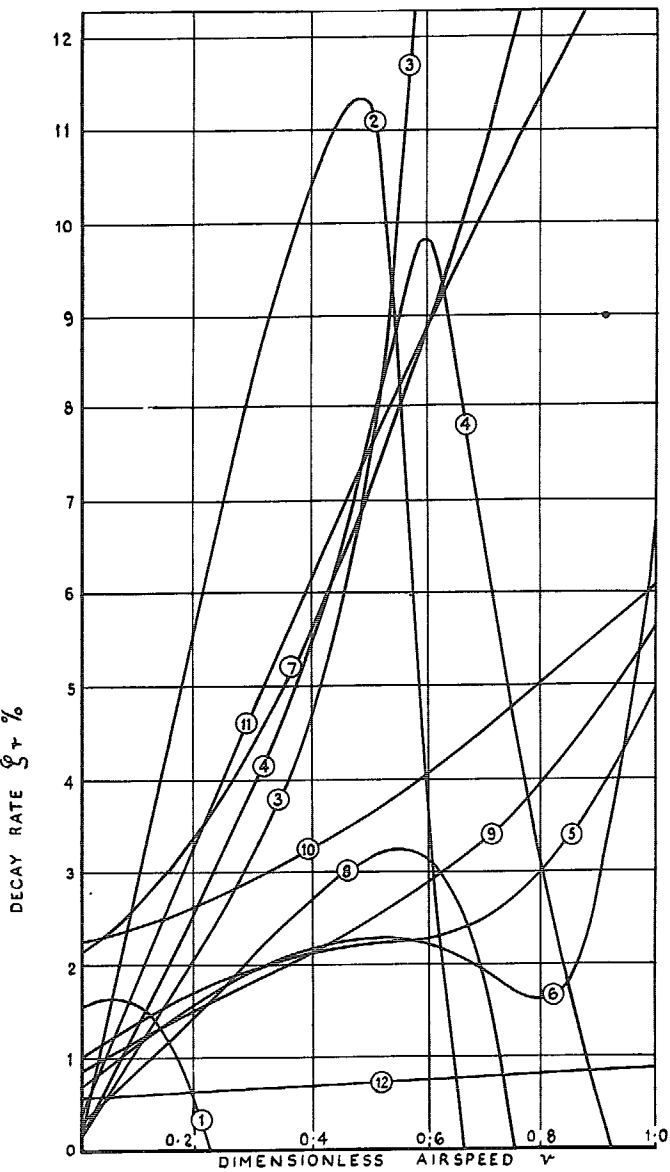


FIG. 22. Flutter of wing with stiffened outboard installation. Decay rate in modes against airspeed.

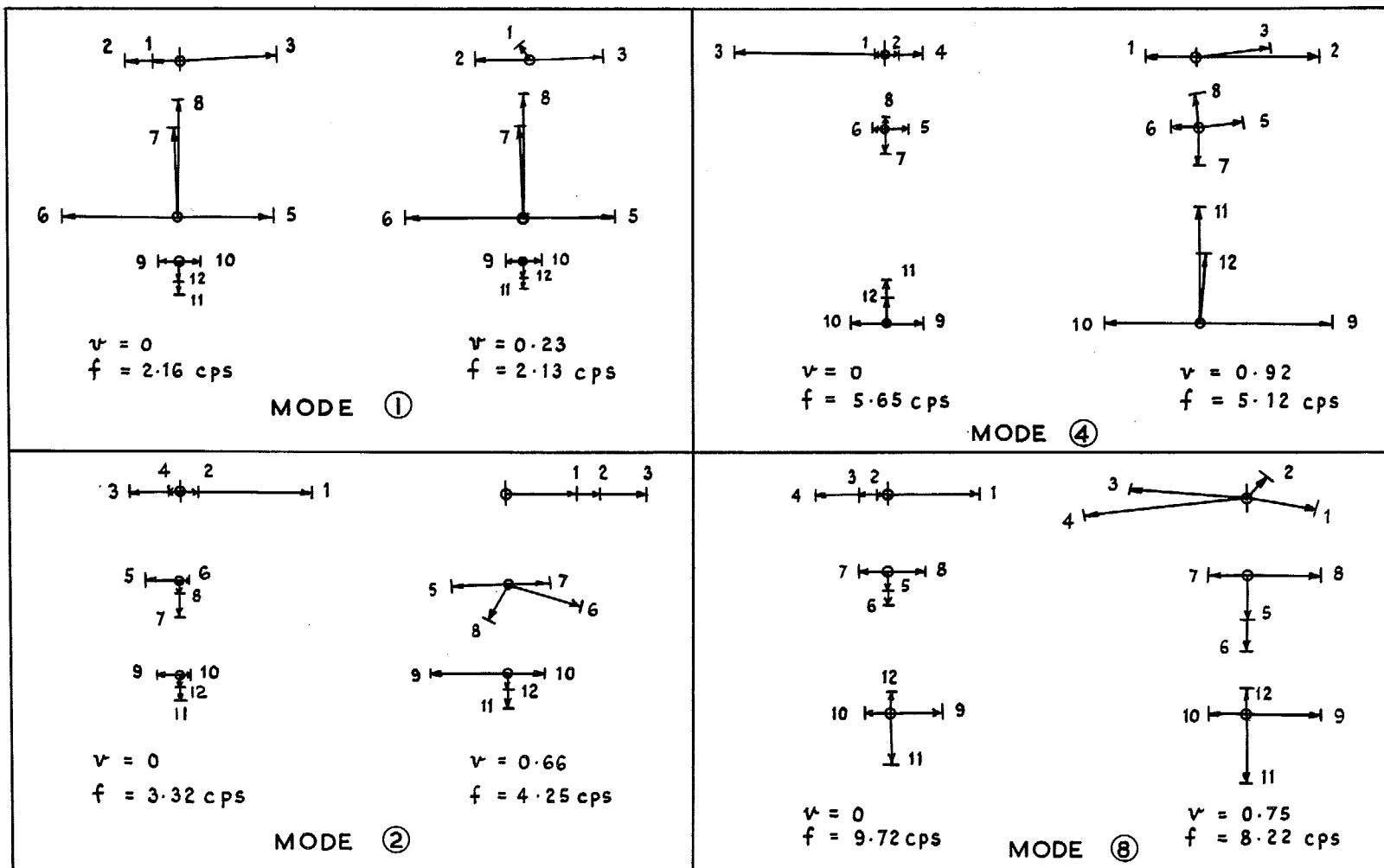


FIG. 23. Unstable - mode vectors for wing with stiffened outboard - engine installation.

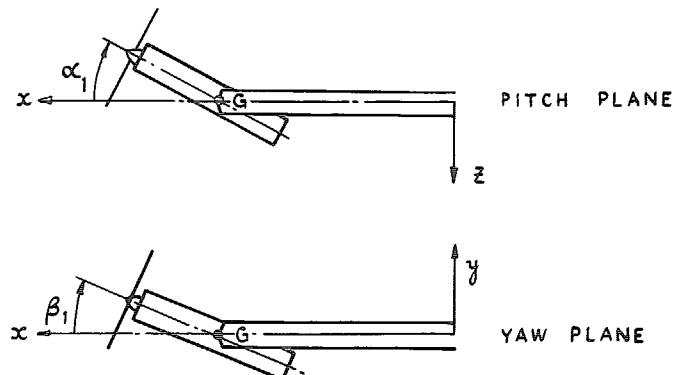


FIG. 24 (a) DISPLACEMENTS IN ENGINE FREEDOMS ONLY

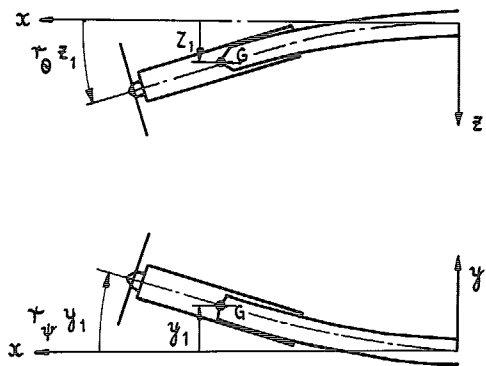


FIG. 24 (b) DISPLACEMENTS IN NACELLE FREEDOMS ONLY

FIG. 24. Displacements of engine - nacelle installation for binary analyses of Appendix A.

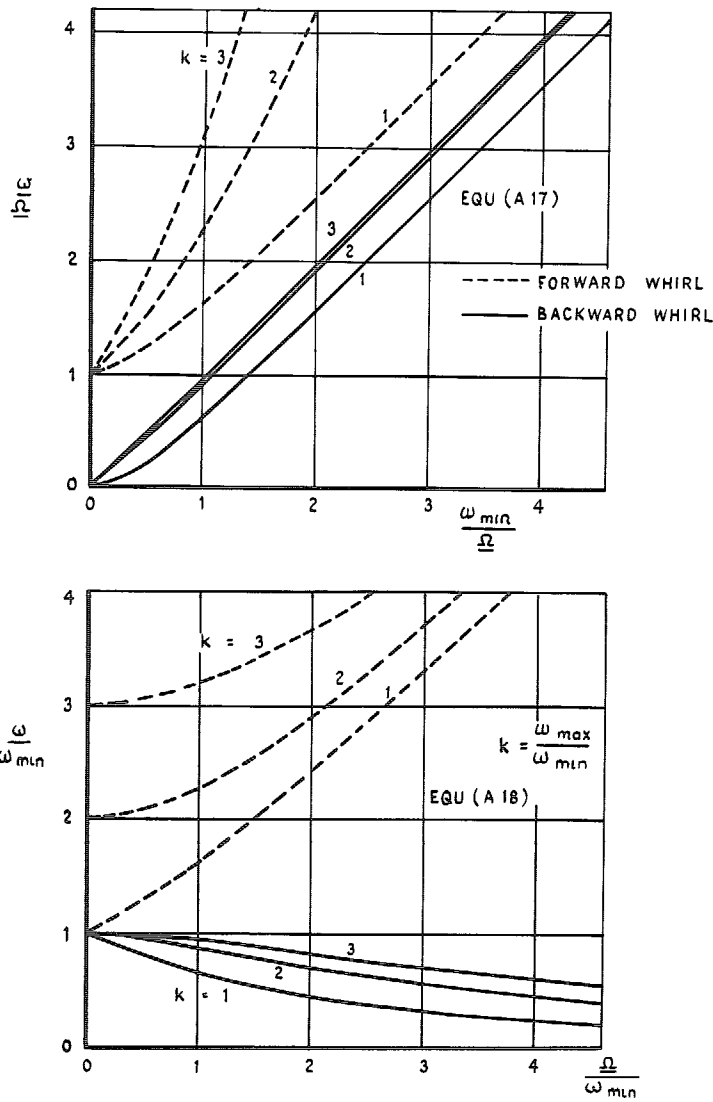


FIG. 25. Theoretical whirl-mode frequencies in 2 degrees of freedom.

R. & M. No. 3536

C Crown copyright 1968

Published by
HER MAJESTY'S STATIONERY OFFICE

To be purchased from
49 High Holborn, London w.c.1
423 Oxford Street, London w.1
13a Castle Street, Edinburgh 3
109 St. Mary Street, Cardiff CF1 1HW
Brasenose Street, Manchester 2
80 Fonthill Street, Bristol 1
288-299 Broad Street, Birmingham 1
7 Linenhall Street, Belfast, B12 8AY
or through any bookseller

R. & M. No. 3536

S.O. Code No. 23-3566